



UNIVERSITÀ  
**ITALO**  
FRANCESE

BLONDEL GUILLAUME

GASNIER THIBAUT

-

5A MECANIQUE ENERGETIQUE

## Gas turbine burner aerodynamic characterization and anemometric measurement



Combustion group

ANNEE 2010-2011

Company tutor: Giulio MORI

Cinzia CIRIGLIANO

University tutors: Alessandro BOTTARO

Azeddine KOURTA

GAS TURBINE BURNER AERODYNAMIC  
CHARACTERIZATION AND ANEMOMETRIC  
MEASUREMENT :

STUDY OF TURBINE BURNERS FOR  
PRODUCTION OF ENERGY

**Thanks :**

We would like first of all to thank the cooperation *L'università Italo-Francese*, the professors Alessandro Bottaro and Azeddine Kourta to have let this partnership possible. We would also want to thank Mr Bottaro for its help to find this Thesis in the ANSALDO company and its support all along the year.

We would also like to thank Giulio Mori, Sergio Rizzo and Cinzia Cirigliano and Giovanna Grosso for their help, integration, availability and advises all along the internship.

We would then wish to thank all the engineering and technical team we worked with along these months spent there : Enrico, Edoardo, Roberto, Cristina, Pietro, Franco.

More generally, we would like to thank all our relatives, friends and all the people we forgot to mention for their support during all this year far away from home.

## Contents

<b>1</b>	<b>Introduction</b>	<b>8</b>
<b>2</b>	<b>The Ansaldo Energia company</b>	<b>9</b>
<b>3</b>	<b>Context and goals of the internship</b>	<b>12</b>
<b>4</b>	<b>The combustion group</b>	<b>13</b>
<b>5</b>	<b>Combustion process and researches</b>	<b>15</b>
5.1	Combustion principles . . . . .	15
5.1.1	Fuel to air ratio . . . . .	15
5.1.2	Flame temperature . . . . .	16
5.2	Combustor design . . . . .	16
5.2.1	Diffusion flame . . . . .	16
5.2.2	Emissions . . . . .	16
5.2.3	Technologies for low pollutant emissions . . . . .	18
<b>6</b>	<b>Characterization</b>	<b>19</b>
6.1	Test bench and measurement system . . . . .	19
6.2	Test campaign . . . . .	21
6.2.1	Set up . . . . .	21
6.2.2	Components . . . . .	23
6.2.3	Flow test procedure . . . . .	23
6.2.4	Outputs data . . . . .	24
<b>7</b>	<b>Anemometric measurement : PIV technique</b>	<b>26</b>
7.1	General frame . . . . .	26
7.2	General principle . . . . .	27
7.3	Procedure for measurement . . . . .	28
7.3.1	The security . . . . .	28
7.3.2	The laser . . . . .	29
7.3.3	The inseeded particles . . . . .	30
7.3.4	The cameras . . . . .	34
7.3.5	Focusing and calibration . . . . .	36
7.4	Setting up the PIV experiment . . . . .	38
7.4.1	Coherence of the experiment with the CFD . . . . .	38

- 7.4.2 The devices and planes of measurement . . . . . 41
- 7.4.3 Transverse section measurement . . . . . 44
- 7.4.4 Longitudinal section measurement . . . . . 46
- 7.4.5 Parameters of the software . . . . . 50
- 7.5 Analysis and results . . . . . 51
  - 7.5.1 The test sequences . . . . . 51
  - 7.5.2 The results and statistical processing . . . . . 52
  
- 8 Conclusion . . . . . 64**
  - 8.1 References . . . . . 65
  
- A Appendix . . . . . 66**

## List of Figures

1	Equation of the combustion Fuel/Air. . . . .	8
2	Combustion process of a flame. . . . .	8
3	Organisation of the Finmeccanica group . . . . .	9
4	Basements of the Ansaldo's power plants in the world . . . . .	10
5	Products of Ansaldo ENERGIA . . . . .	11
6	Organization chart of the combustion group. . . . .	13
7	NOx formation. . . . .	17
8	View of the bench test. . . . .	20
9	pressure outputs . . . . .	22
10	Atomizer which creates droplets. . . . .	26
11	Three measurement velocity methods. . . . .	27
12	Laser radiation. . . . .	29
13	Time of response of a particle under deceleration in function of its diameter. . . . .	32
14	Light scattered by an oil particle in an air flow. The scales are the same. . . . .	33
15	Principle of a Laskin Nozzle. . . . .	34
16	Similitude human vision with PIV 3D. . . . .	34
17	Image seen by the camera and aperture angles. . . . .	35
18	The two cameras with an inclination angle respect to the measurement plane. . . . .	37
19	Target set at the place of the measurement plane. . . . .	37
20	Calibration grids generated by the software. . . . .	38
21	The two different planes of measurement chosen for the PIV. . . . .	42
22	Measurement line for PIV experiment. . . . .	43
23	Constitutive pieces of the liner. . . . .	43
24	Layout for the transverse PIV. . . . .	44
25	Target ready for calibration at the place of the measurement plane. . . . .	45
26	Horizontal perspective seen by the crossed zone of the two cameras. . . . .	45
27	Vertical perspective seen by the crossed zone of the two cameras. . . . .	46
28	Layout for the longitudinal PIV. . . . .	47
29	Laser and target set up. . . . .	47
30	View of the target position and of the overall layout of the cameras (symmetric on the right picture). . . . .	48
31	Camera snapping into the test section. . . . .	49
32	The further the camera is, the largest will be the measurement plane intercepted. . . . .	49

33 Images capturing sequence for one camera. Note : t is the starting time of the experiment,  $\Delta t$  correspond to the previously defined “Time between pulses” linked to the flow velocity and n to the “Number of images” to acquire. . . . . 51

34 Image captured by the software. . . . . 53

35 Background isolated. . . . . 53

36 Isolated illuminated particles represented by this cloud in the center. . . . . 54

37 Cross correlation obtained for a couple of images and for each camera at the same time. 55

38 Moving average validation for each camera at the same time. . . . . 56

39 Stereo PIV Processing with and without the cleaned cross correlation. . . . . 56

40 Mean representation of the flow recorded a certain time. . . . . 57

41 3D average maps along the two measurement planes for  $\dot{m} = 1.012$  kg/s. . . . . 58

42 3D average maps along the two measurement planes for  $\dot{m} = 1.442$  kg/s. . . . . 59

43 3D average maps along the two measurement planes for  $\dot{m} = 1.62$  kg/s. . . . . 60

44 Transverse average maps for the three air mass flow rates. . . . . 60

45 Longitudinal average maps for the three air mass flow rates. . . . . 61

46 Profile plot of the velocity W for the transverse measurement. . . . . 61

47 Profile plot of the velocity V for the longitudinal measurement. . . . . 62

48 Overlaying of the swirler with the trasverse vectorial map. . . . . 63

**List of Tables**

1 Indicative values of the NOx emissions expressed in ppmvd, 15% O<sub>2</sub>, as NO<sub>2</sub>, relative values for a gas turbine with natural gas. . . . . 18

2 Main characteristics of the laser. . . . . 29

3 Seeding materials for gas flows. . . . . 30

4 Main features of the two used objectives. . . . . 36

5 Mass flow rates to fix to have similitude CFD/PIV experiment. . . . . 41

6 Mass flow rate used in function of the similitude criterion. . . . . 51

## 1 Introduction

The global warming is in part due to atmosphere pollution. Pollution which is mainly caused by emission of harmful particles from factories, power plants and vehicles. In fact, to produce, provide energy and move we are still dependent on energetic systems which run with fuels.

The combustion process as we all know consists in the chemical reaction between a combustive and a fuel (see Figure 1 below) which creates heat, light and products (see Figure 2 below). Among these products, there are some which are harmful for nature. As it is strictly impossible to vanish them all, the research and industry have to find a way to reduce them as much as possible.

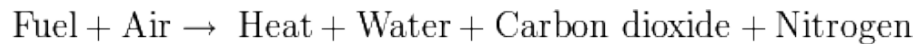


Figure 1: Equation of the combustion Fuel/Air.

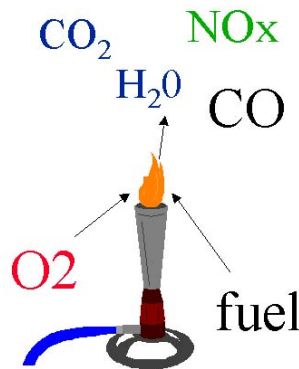


Figure 2: Combustion process of a flame.

Among these products, there are  $\text{CO}_2$ ,  $\text{H}_2\text{O}$ ,  $\text{CO}$  or even  $\text{NO}_x$ . The goal of this Thesis/Internship in the Ansaldo Energy company will be to study the used and developed burners and particularly their aerodynamic characteristics which are one of the main factors which impact on the combustion efficiency. With the final objective of reducing the harmful particles emission and so to produce a "cleaner" energy together with an efficient combustion.

In a first part, we will present the story and the activities of the Ansaldo company. Then the devices we worked on during the period. After that we will describe the work performed during the first part of the internship concerning on: the characterization of a burner. Finally, we will expose the technique used to study the flow field which get out of the burner: the Particle Image Velocimetry.

This document has been realized with *LateX* (pronounced /la.tek/), a freeware allowing a simple and precise layout of text documents. It is mainly used in the edition of scientific documents (publications, articles, reports).

## 2 The Ansaldo Energia company

Ansaldo Energia is a Finmeccanica Company, Italy's leading high technology group and a major player worldwide.

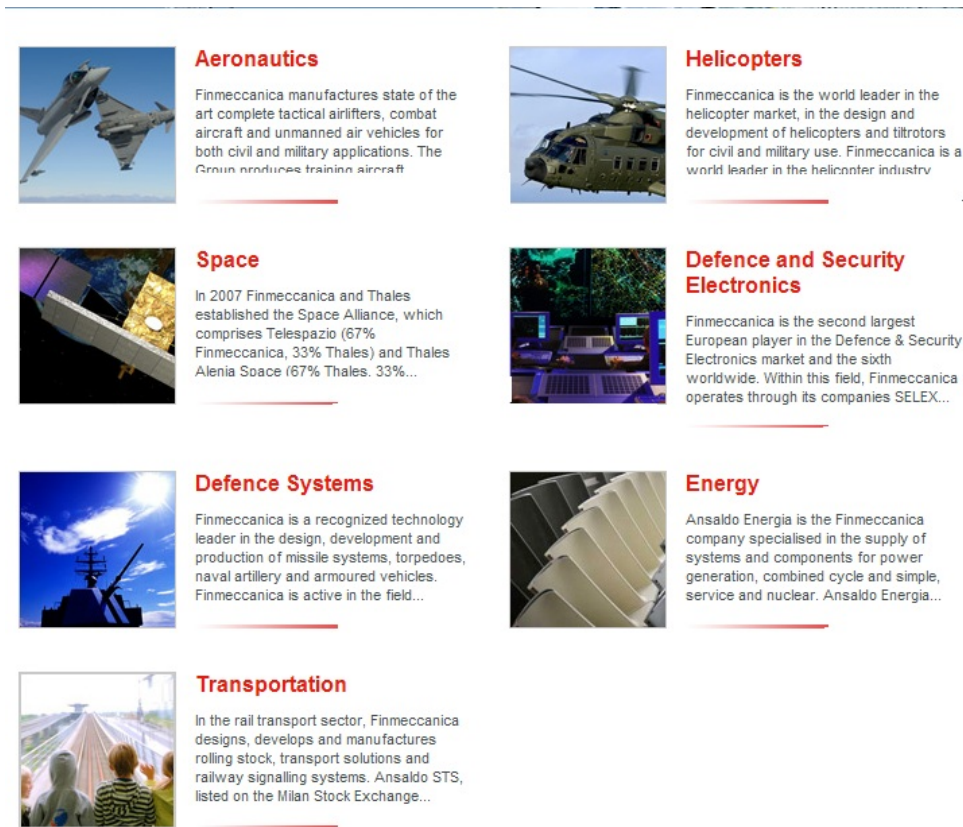


Figure 3: Organisation of the Finmeccanica group

Ansaldo Energia is Italy's leading producer of thermoelectric power plants, operating on international markets for customers ranging from Public Administration to Independent Power Producers and Industrial Clients. Since 1853, Ansaldo has proved its know-how in the energy field, it has constantly responded to the international market by innovations, organization, design and construction skills.

Over the years the company has made significant contributions to the key mechanical, naval and electrical engineering sectors. At present, Ansaldo Energia, employs about 2200 people, 900 of whom are factory workers and 1300 are office workers. The firm has multiply its competences in many energy fields such as the nuclear, fuel cells...

- Ansaldo Energia
- Ansaldo Nuclear
- Ansaldo fuel cell

- Ansaldo ESG
- Ansaldo Thomassen

Ansaldo Energia has excellent credentials, with an installed capacity of over 170,000 MW in more than 90 countries. The Company's main points of strength are its comprehensive offering and a flexible approach to projects. Ansaldo Energia has completed more than 1,700 projects throughout the world, featuring a broad range of solutions and with the company acting in various roles.

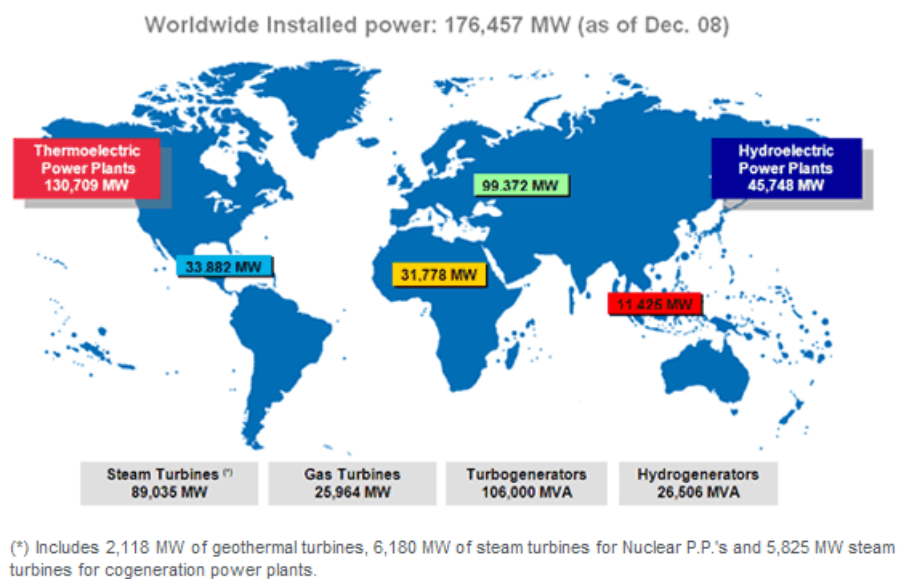


Figure 4: Basements of the Ansaldo's power plants in the world

Ansaldo Energia offers the power generation market a broad range of products and services with the support of its independent manufacturing capabilities. From component design and construction through to comprehensive turnkey solutions; all delivered to the highest possible quality standards. Ansaldo Energia creates and works for responding to the needs of its customers in terms of efficiency, reliability and environmental impact.

The energy systems produced by Ansaldo Energia respect the aim of meeting specific personalization requests.

## PRODUCTS



### Plants - Ansaldo Energia

Complete plants for energy generation, combined and open cycles, conventional, cogenerative and geothermal. Power up to 825 MWe with efficiency up to 58%. More than 177,000 MW of power...



### Gas turbines - Ansaldo Energia

From 70 to 294 MW of power, three gas turbines models, AE64.3A, AE94.2, AE942K, AE94.3A, featuring advanced technological solutions and designed to satisfy clients' requirements in...



### Steam turbines - Ansaldo Energia

From 40 to 1000 MW of power, the production covers the entire range of applications for the generation of fossil fired cycles, combined cycles, cogeneration steam turbines for...



### Generators - Ansaldo Energia

Production of both turbo-generators and hydro-generators, all designed to satisfy the most demanding customer requirements in terms of efficiency, reliability and environmental impact...

Figure 5: Products of Ansaldo ENERGIA

We will explain now the goals of this internship.

### 3 Context and goals of the internship

In the research and development group a dual approach calculation/experimentation is realized. In our case, the PIV experimentation has been done on the new generation of burner in sort of reducing the NO<sub>x</sub> emission. It is necessary to know and understand the dynamic flow motion of the burner, then a numerical and experimental procedure is undertaken.

It is a tough work which require a specific collaboration between the technical, numerical and experimental part.

The combustion group studies different types of burner either doing atmospheric measurement of the pressure drop with an imposing flow rate or either by measuring the flow field using optical techniques. It was the two parts of our work during the training course in the experimental combustion group.

People have always been interested in the comprehension of the physical flow phenomenon. There is a lot of methods for understanding the behavior of the flow through every type of geometry. A century after PRANDTL's experiments (1904), it's easily possible to extract quantitative information about the instantaneous flow velocity field. Indeed, with the great evolution of the technology, we are able to visualize the flow field resulted in a vector map of the instantaneous velocity field. The visualization method we have used is the Particle Imaging Velocity whose we will describe its principle of working.

## 4 The combustion group

### Numerical and experimental sections:

The combustion group is divided in two sections, the experimental section and the numerical section, which work together for the same goal. They focus their work on the natural gas distribution in combustion near field for the reduction of the NOx emissions, the flame shape for the study of the combustion dynamic analysis or the near field heat transfer for the study of the combustor integrity, or also for the acoustic phenomena which can occur during the combustion process (humming).

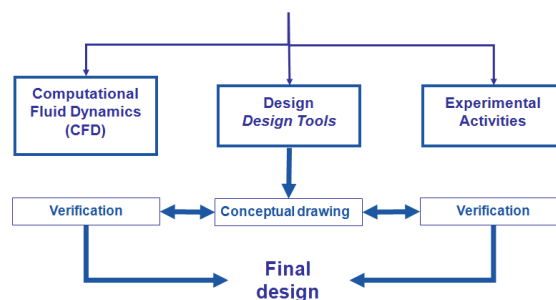


Figure 6: Organization chart of the combustion group.

### Numerical section:

The numerical group uses CFD (Computation fluid dynamics) codes or the developed tools of the company. Ansaldo has increased its knowledges and its database about the combustion process (thermodynamic and reaction mechanisms). They has developed skills in the humming phenomenon, it can manage with parameters (geometrical, aerodynamic of the system and the operative parameters.)

- CFD codes (FLUENT, MathCAD,ICEM)

#### Tools developed by Ansaldo:

- Chemical Reactor Model (CRM) (Emissions (NOx, CO))
- Pressure Loss Model (PLM) (Burner design)
- Data base (Thermodynamic and kinetics)
- Thermo-acoustic model (Humming)
- Other tools

### Experimental section:

The experimental section can perform different kind of tests regarding to combustion systems, at ambient conditions. It has available a wind tunnel and multiple optical techniques.

1. Wind tunnel 8'000  $m^3/h$  An atmospheric air wind tunnel equipped with a controlled, variable speed blower; maximum flow rate 10'000  $m^3 / h$  (eq. to 2.7 kg/s); maximum pressure drop 16'000 Pa. Dedicated mass flow meter and pressure drop measurements.
2. Wind tunnel 6'000  $m^3/h$  An atmospheric air wind tunnel equipped with a controlled, variable speed blower; maximum flow rate 6'000  $m^3 / h$  (eq. to 2.0 kg/s); maximum pressure drop 10'000 Pa. Dedicated mass flow meter and pressure drop measurements.
3. Wind tunnel pressurized air feed Each one of the wind tunnels can be fed with pressurized air, maximum ratings 600 kPa and 150  $m^3 / h$  (eq. to 0.050 kg/s). Dedicated mass flow meter and pressure drop measurements are also provided.
4. Laser Doppler Velocimetry At the outlet of any of the wind tunnel a flow measurement based on CW laser may be applied. LDV system is able to measure air speeds up to 50 m/s in a 1 mm x 0,2 mm x 0,2 mm volume, that can be displaced at will in a 500 x 500 x 1500 mm investigating volume.
5. Particle Image Velocimetry At the outlet of any of the wind tunnel a flow measurement based on double, twin pulsed lasers may be applied. PIV system is able to measure flow fields in a plane of approx. 200 mm x 200 mm x 1mm for air speeds up to 80 m/s.

## 5 Combustion process and researches

Improving the cycle efficiency while reducing emissions has always been the main work for the gas turbine designers, it is a big challenge because of the difficulties linked to the principles of the formation of the NOx. Indeed higher is the fluid temperatures, higher is the efficiency but also it promotes the NOx formation. Furthermore, reducing available oxygen to reduce NOx can result in higher carbon monoxide (CO) and unburned hydrocarbon emissions due to incomplete combustion. A Balance between the whole parameters has to be done in sort of having a better efficiency always responding to the pollutants request.

### 5.1 Combustion principles

Flame is a self-sustaining propagation of a localized combustion zone at subsonic velocities.

We can characterizes two classes of flames, premixed and non-premixed (or diffusion) related to the state of mixing of the reactants:

- **Premixed flames:** fuel and oxidizer are mixed at the molecular level prior to the occurrence of any significant chemical reaction.
- **Diffusion flame:** the reactants are initially separated, reaction occurs only at the interface between the fuel and oxidizer, where mixing and reaction both take place.

Turbulent non premixed flames are employed in the majority of practical combustion system, we know very well about the control of this type of flame.

#### 5.1.1 Fuel to air ratio

A significant parameter used to characterize combustion is the fuel to air ratio ( $f/a$ ), expressed either on a volume or mass basis.

With precisely enough air to theoretically consume all of the fuel, combustion is referred to as having a "stoichiometric"  $f/a$  ratio. Adding more air produces combustion that is fuel-lean, and adding less air produces combustion that is fuel-rich. Because differing fuels have different stoichiometric  $f/a$  ratios, it is convenient to normalize the  $f/a$  ratio by the stoichiometric value, producing the term equivalence ratio  $\phi$ :

$$\phi = \frac{(f/a)_{actual}}{(f/a)_{stoich}} \quad (1)$$

By referring to the equivalence ratio, combustion using different types of fuel is readily described as lean if  $\phi < 1$  or rich if  $\phi > 1$ .

### 5.1.2 Flame temperature

Another important combustion parameter is the flame temperature. It differs with the species which occur during the combustion process. The highest flame temperatures would be produced at  $\phi = 1$ , because all of the fuel and oxygen would be consumed. In practice, the effects of species dissociation and heat capacity shift the peak temperature to slightly above stoichiometric ( $\phi \approx 1.05$ ). It is an important parameter because the higher the flame temperature is, higher is the efficiency of the cycle but there is a peak of the NOx production at high temperatures.

## 5.2 Combustor design

### 5.2.1 Diffusion flame

In diffusion flame combustion, both fuel and oxidizer are supplied to the reaction zone in an unmixed state. The fuel/air mixing and combustion take place simultaneously in the primary combustion zone. This generates regions of near-stoichiometric fuel/air mixtures where the temperatures are very high.

Because the flame stability of a diffusion flame is very good, it has been adopted for combustor systems and can operate over a wide range of equivalence ratios. The disadvantage of this type of combustion is the high temperature in which the formation of NOx occurs. Different type of combustors have been developed in sort of reducing the pollutant emissions.

### 5.2.2 Emissions

The primary pollutants emitted by gas turbine engines are NOx, CO and unburned hydrocarbons (UHC). Sulfur dioxide, particulate matter (PM) and trace amounts of hazardous air pollutants may also be present when liquid fuels are fired.

Pollutants affect our environment and human health in many ways:

- Altered properties of the atmosphere and precipitation
- Harm to vegetation
- Soiling and deterioration of materials
- Potential increase of sickness and mortality in humans

### NO<sub>x</sub> formation:

There are two mechanisms by which NO<sub>x</sub> is formed in gas turbine combustors:

1. The oxidation of atmospheric nitrogen found in the combustion air (**thermal NO<sub>x</sub> and prompt NO<sub>x</sub>**): Thermal NO<sub>x</sub> production rates fall sharply as either the combustion temperature decreases.
2. The conversion of nitrogen chemically bound in the fuel (**fuel NO<sub>x</sub>**):

Fuel NO<sub>x</sub> is formed when fuels containing nitrogen are burned. When these fuels are burned, the nitrogen bonds break and some of the resulting free nitrogen oxidizes to form NO<sub>x</sub>. With excess air, the degree of fuel NO<sub>x</sub> formation is primarily a function of the nitrogen content in the fuel.

### CO and UHC formation:

Both CO and UHC are the products of incomplete combustion. Given sufficient time and at high enough temperatures, these two pollutants will be further oxidized to carbon dioxide and water.

Turbine manufacturers have significantly reduced CO emissions from combustion turbine by developing lean premix technology.

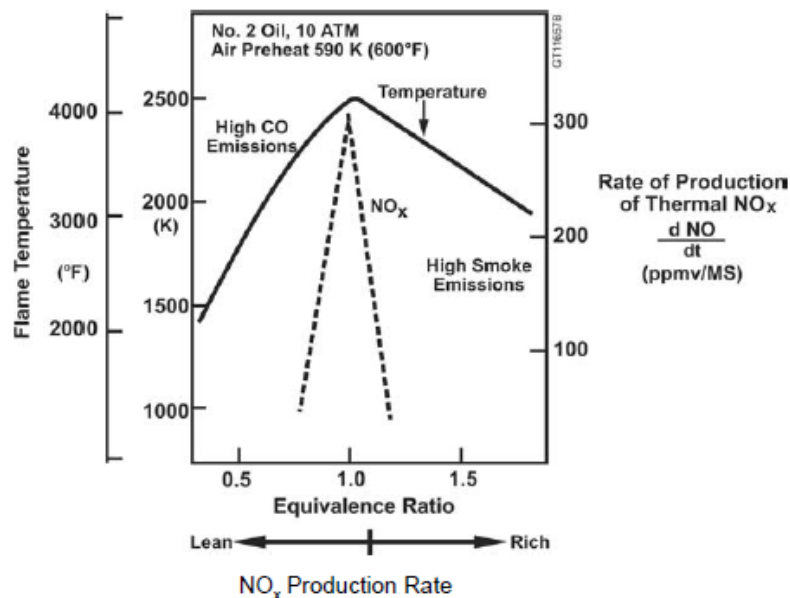


Figure 7: NO<sub>x</sub> formation.

### 5.2.3 Technologies for low pollutant emissions

In the early 1970's, when we start to want to control the emissions, we focused on the NO<sub>x</sub> rate. Injection of steam or water into the combustion zone produced the required reduction in NO<sub>x</sub> emissions with minimal performance impact. A lot of technologies have been developed to achieve lower pollutant emission rates, improving the combustion process:

- Wet controls (water or steam injection)
- Dry combustion controls (lean combustion, reduced residence time, lean premixed combustion, and two-stage rich/lean combustion: see references [5] )
- Catalytic combustion
- Rich Quench Lean Combustors
- CO oxidation catalysts

The continuous combustion of a gas turbine combustor simultaneously offers both low NO<sub>x</sub> and low CO/HC emissions, and the combustion technology does not require an exhaust after treatment device which is very expensive and bulky.

Another technology has been developed which offers a means of achieving both low NO<sub>x</sub> and low CO emissions.

This table refers to the reduction of the NO<sub>x</sub> emission rates with the last technologies still studied.

from UE 2001/80/CE directive about emissions (to reach in january 2008)	25 ppm
emission with diffusion combustor	200 ÷ 300 ppm
emissions with water/steam injection	40 ÷ 60 ppm
emissions with DLN, guaranteed values	15 ÷ 25 ppm
reached emissions with advanced DLN	9 ÷ 15 ppm

Table 1: Indicative values of the NO<sub>x</sub> emissions expressed in ppmvd, 15% O<sub>2</sub>, as NO<sub>2</sub>, relative values for a gas turbine with natural gas.

Emissions levels are expressed in many different ways; differences arise from the needs of different technologies, per example for automobile, they are expressed in grams-per-mile, and many measurements are reported as parts-per-million (by volume).

## 6 Characterization

In the first part of the training course we have done aerodynamic flow characterization tests of various components in order to know the effective area of passage, by measuring the pressure drop of the specific passage with respect to various conditions of air flow at ambient conditions, so in case of atmospheric temperature and pressure. The imposed conditions of flow rate or pressure ratio have been provided by criteria of scaling respect to hot conditions (real combustion and operating pressure conditions).

Results can be used also for comparison and validation of the numerical modeling work (CFD).

All the flow tests will be performed with air, for all the passages, at ambient temperature and pressure. The required pressure ratio ( $p_i/p_o$ )(inlet pressure/outlet pressure) will be imposed. Then, the resulting condition of air inlet flow rate, air inlet temperature, atmospheric pressure and pressure drop at the specific component will be recorded.

All of these results will be controlled and with a post procedure we will determine the effective flow area which is confronted to the CFD results. It can be plot the pressure ratio in function to the effective flow area.

### 6.1 Test bench and measurement system

The test bench is used for the flow characterization of the combustion system.

The inlet air is sent by a fan through the pipe provided with the primary element for the monitoring of the inlet air flow rate and temperature. The inlet air goes into a cylindrical plenum that ends with a plane surface provided of threaded holes in order to mount the component by means of interfaces flanges. The air outlet from the component ends at atmospheric conditions.

We had in disposition two different flow test benches, it had been chosen the Linea 10000, which can work until 10 000  $Nm^3/h$ . ( $\approx 3,2$  kg/s) because we deal with high flow rate and it has been adapted to our components.

The flow test bench (see Figure 8 below) works by the way of a centrifuge electro-air-fan which works from 12000  $m^3/h$  and 14000 Pa of prevalence. It allow to have a variable flow rate in a continuous mode through the regulation of the rotation speed of the motor. As it is shown on the scheme, air arrives from the air-fan and air gets into a duct ( $\phi 10'' = 273$  mm thickness 3 mm) to a cylindrical air box of dimensions: 1500 mm of length and 875 mm of diameter, where it will be inserted our test

component.

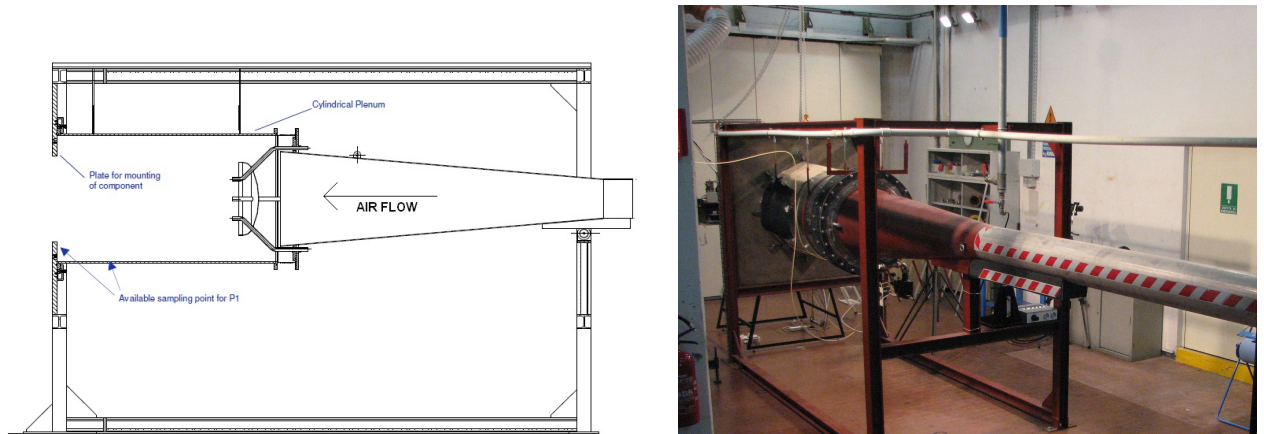


Figure 8: View of the bench test.

The experimental circuit ' LINEA 10000 ' is provided with the following instrumentation:

1. A regulation system for the rotation speed of the electro-air-fan for a air flow rate variation in a continuous mode.
2. A air flow measurement system which is used for a range of measurement:  $18 \div 8000 \text{ Nm}^3/\text{h}$ , for different calibrations valid for these scale offsets:
  - Scale offset 1:  $500 \text{ Nm}^3/\text{h}$
  - Scale offset 2:  $3000 \text{ Nm}^3/\text{h}$
  - Scale offset 3:  $8000 \text{ Nm}^3/\text{h}$

Accuracy:  $\pm 1 \%$  of reading value  $\pm 0.5 \%$  full scale per single range

And a thermocouple for the measurement of the air temperature.

A relative pressure output in the air box for the measurement of the  $\Delta P$  respect to the air atmospheric pressure and a differential pressure transmitter with a range of 400.000 mbar. - Min. Span: 4.0 mbar - Accuracy:  $\pm 0.04 \%$  FS

Compressed air line: Inlet air flow rate and temperature: mass flow transmitter:

- Range of measurement: 0.2328 145.96 g/s
- Calibrated for 3 different ranges: 0 34, 34 351, 351 930 kg/h
- Accuracy:  $\pm 1\%$  of reading value  $\pm 0.5\%$  full scale per single range

- Output signal: 4-20 mA.

A burner ANSALDO for gas turbine application which is inserted in a air box.

## 6.2 Test campaign

### 6.2.1 Set up

In order to characterize the interested section, we had to find some tools to obstruct the air passage if we want to know the effective flow area. Tape has been set just to remain the transit of the flow in the interested components. Then pressure outputs were installed all over the different sections, we want to know the pressure between downstream and upstream. Knowing the pressure inside the air box located upstream, reading on the manometer the pressure downstream, the  $\Delta P$  will be given, to finally get the effective flow area.

In our campaign, we had to determine the effective area for different air passages for an Ansaldo's burner which had been subjected to some modifications.

This is a scheme of our system with the different parts which have been flow tested. According to the parts that we want to isolate we have to link the pressure outputs to the differential pressure transmitter in order to read the pressure downstream and upstream. The unique combination of several sensor systems in a single device allows simultaneous measurement of differential pressure and absolute pressure. We had to pay attention to collect it in the right way to have a positive lecture of the pressure (For example, if we want to link the pressure between P1 and P2, it won't be the link same as P2 and P4).

We needed also to take another differential transmitter which enter in a major range of pressure to avoid entering in the full scale of the system.

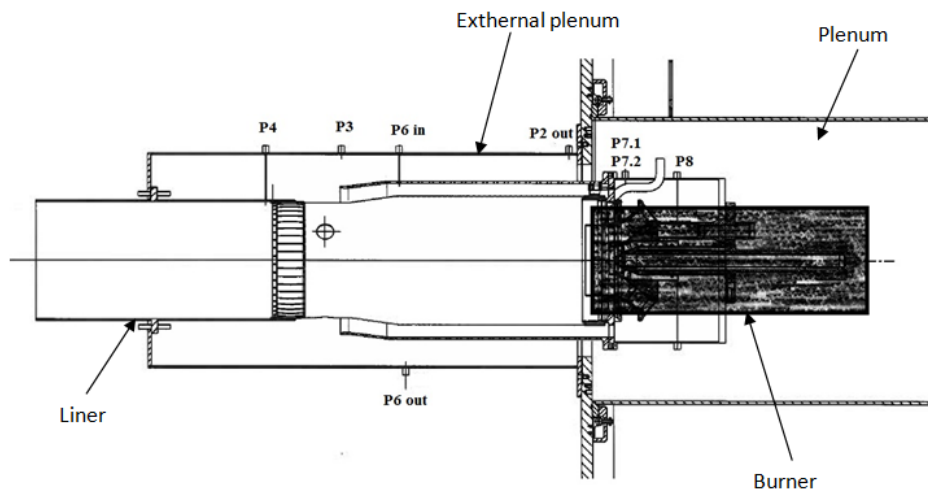


Figure 9: pressure outputs

Some pressure outputs had been set in order to allow the characterization of the interested components:

1.  $P_1$ : air box pressure;
2.  $P_2$ : pressure immediately downstream of the flange;
3.  $P_3$ : pressure immediately downstream of the dilution hole;
4.  $P_4$ : pressure immediately upstream of the hula seal of the liner;
5.  $P_5$ : pressure immediately upstream of the flow sleeve holes of the flange;
6.  $P_6$ : pressure corresponding of the last hole of the flow sleeve;
7.  $P_7$ : Pressure set at the beginning of the end cover dummy (double media out).

### 6.2.2 Components

The first burner studied is settled inside an annular combustion chamber with 24 others burners to provide the quantity of electricity wanted.

Information we can extract from these "cold combustion" flow tests will be useful to for the pressurized combustion tests that will be performed afterwards.

Flow tests realized at the combustion group of ANSALDO ENERGIA will bring some information about the flow area of our different components, that is to say, the regulation of the quantity of combustibile to have the best combustion configuration to furnish the energy needed.

Guaranty a minimized emission of pollutants with the quantity of energy is what the customer expects.

### 6.2.3 Flow test procedure

For each component flow tested, we apply a flow test procedure:

We assembly the component under investigation, with adhesive tape and/or dedicated tools we close any air passage that has not to interfere with the measurement. After checking and fixing eventual leakages, the test can be started.

$P_{atm}$	$P_{ratio}$	$\Delta P$ wanted	$\Delta P_{offset}$ display	$\Delta P$ (Pa)	$\Delta P$ display	$P_{upstream}$ display
-----------	-------------	-------------------	-----------------------------	-----------------	--------------------	------------------------

The reference conditions of all the instruments (eventual offsets) together with the atmospheric pressure were recording before inletting the air flow rate. Indeed, we want to impose the pressure ratio, which is the  $\frac{P_{upstream}}{P_{downstream}}$ .

We can obtain the  $\Delta P$  wanted :

$$\Delta P_{wanted} = (P_{ratio} - 1) \times P_{upstream} \quad (2)$$

$$\Delta P_{offset} = \Delta P_{offset display} \times full\ scale\ (40\ 000\ Pa) \quad (3)$$

$$\Delta P_{display} = \Delta P_{wanted} + \Delta P_{offset} \quad (4)$$

We control by an inverter the centrifuge air-fan and reading all the data directly on the interface of the display, we could increase the inlet air flow rate up so to reach the  $\Delta P$  corresponding to the specific pressure ratio. Depending on the turbulences, we have to find a flow stability point. For each pressure ratio reached, once the regime conditions has been verified, all the required date are recorded

for about 3 minutes. During the post processing the reliability of the flow test is checked by verifying the data variation that has to be within 3% of the desired value.

The test data are recorded by a dedicated PC (inlet air flow rate; inlet air temperature; inlet component air pressure; ambient pressure, at component discharge) with a sampling rate of 1 kHz and a recording rate of 10 Hz, the recorded data are saved as ASCII files.

Pressure upstream and downstream can be read on the computer via the acquisition system.

- Input data
- Output data (inlet air flow rate, inlet air temperature, inlet component air pressure, ambient pressure )

Characterization process is not as simply as it could be. Indeed, it depends a lot on the geometry of the component to be tested. Individualize the different parts of the components is not possible every time and pressure outputs have to be installed in a strategic point to characterize as better as possible the components.

We have been faced with some difficulties during the flow tests because the results obtained did not correspond to the flow rate expected. When we input the pressure ratios, we expected air mass flows given by the CFD. At this point, we can ask wonder where comes from of our error (leakage in some parts of the flow line, pressure outputs, problem on the measuring system...). The errors that we have seen, was either a leakage due to the soldering or the pressure output which has been placed in an area of the component where we have recirculation, and the pressure read was the dynamic pressure.)

#### 6.2.4 Outputs data

- Test Pressure Ratio
- Air flow Rate (W) in kg/s
- Inlet Total Pressure (P1) in kPa
- Inlet Total Temperature (T1) in °C
- Barometric (ambient) Pressure (P2) in kPa
- Mass Flow Parameter, MFP, in kg/s
- Flow Effective Area, Aeff, in mm<sup>2</sup>

Fluid properties:

For the different pressure ratio, we will obtain a different effective flow area, which increases until saturation of the parameters. Neglecting the nozzle losses for an ideal gas and the effect of its mass, we can obtain the velocity of the adiabatic discharge.

With the SAINT VENANT formulas we find the effective flow area:

$$\alpha A = \frac{Q_{mis}}{\sqrt{(2 \times (\gamma/(\gamma - 1)) \times \rho) \times P_{upstream} \times \left( \frac{P_{atmospheric}^{2/\gamma}}{P_{upstream}} \right) - \left( \frac{P_{atmospheric}^{\gamma/(\gamma-1)}}{P_{upstream}} \right)}} \quad (5)$$

- $\alpha A$ : effective flow area [m<sup>2</sup>];
- $Q_{mis}$ : mass flow rate measured [m<sup>3</sup>/s]
- $\gamma = C_p/C_v = 1,4$  [adim];
- $\rho$ : density of the fluid (air) [kg/m<sup>3</sup>]
- dynamic viscosity =  $1,7894 \cdot 10^{-5}$  [kg/m.s];
- molecular weight = 28,9644 [g/mol]

This part of the work need a lot of accuracy during the flow test campaign, actually the results obtained by these tests can be used for comparison with CFD or to give parameters to the calculation tools or to give information for the test performed with real combustion (actual temperature and pressure condition) made with the purpose of verifying performances and efficiency of the developed component.

## 7 Anemometric measurement : PIV technique

### 7.1 General frame

As we said in the introduction, the combustion process is a very tough and articulated field of research. It follows the simple equation of the conservation of the species for which nothing appear, nothing disappear and everything get transformed. However among the products of this equation some of them are harmful for health and environment and represent a source of pollution for the environment. To struggle against them and reduce their quantity we can play with many parameters such as the composition of the reactant, the thermophysical conditions in which the reaction will occur or even the quality of the mixing between the different reagents. Let's focus on that last point. In fact the quality of a combustion process will depend a lot on the homogeneity of the mixing fuel/combustive. The fuel (in its liquid form) is injected and sprayed into the combustion chamber by the way of atomizer (see Figure 10 below) which break up the liquid into droplets. The smaller the droplets will be the better will be the combustion process. After that, this fuel cloud has to be homogeneously mixed with the combustive. We will detail in this chapter how it is done for a particular device : a swirler. This device has the goal to create a tangential component to the velocity in order to create a vortex and small vortexes. It is also equipped with some holes created to carry fuel nozzles. These nozzles will not be present during our experiment. Not any photo of the component will be shown because for the confidentiality of the project.



Figure 10: Atomizer which creates droplets.

To control this homogeneity, many techniques can be used. Among them, the Particle Image Velocimetry (PIV) which allows to see how the vortical structures evolve in space and time through the quantity of motion field.

In this part, we will explain the main principle of the PIV, the security linked to the measurement, the different measures done and finally the results will be presented.

## 7.2 General principle

It exists different velocimetry measurements depending on what the user wants to measure (study the flow motion or simply get its velocity). The three main techniques usually used can be classified in two categories :

- optical measure (indirect measure);
- direct velocity measure.

Among the optical methods we can name the Laser Doppler Velocimetry (LDV) and the Particle Image Velocimetry (PIV). Their main advantage is that they don't interfere with the fluid (in fact, just a laser light go trough the fluid in motion). On the contrary, for the direct velocity measures (such as the hot wire) a probe has to be inserted into the flow motion which can tend to modify its behavior. We will just focus on the PIV method.

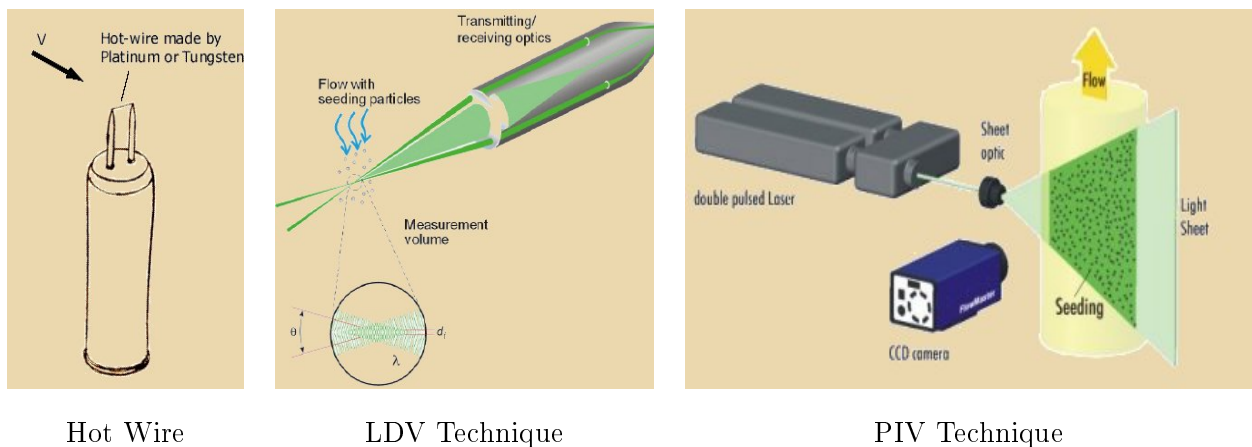


Figure 11: Three measurement velocity methods.

More particularly, the specificity of the PIV compare to the two other techniques of velocity measurement (hot wire or LDV) is that we can get the flow structure for two components of the velocity field (2D PIV). And the most interesting is that we can also get it for the third component of this field (called 3D PIV or stereoscopic PIV). This method is not very accurate to compute the velocity but it allows to see the velocity field and mostly the vortex or recirculating structures within a flow. The principle is the same for both techniques but the 3D needs two cameras (instead of one for the 2D PIV) in order to snap pictures of the flow from two different viewing angles to create a perspective. We will explain the principle further. In that report, we will just focus on the 3D PIV, which is the one we worked with.

The PIV technique consists in measuring the velocity field of a fluid by taking two pictures triggered within a very short time with a high sensor resolution camera. Then comparing these two pictures thanks to statistical tools (cross-correlation for example) we can extract the mean displacement of the particles within the plane measurement taken by the camera. The more the user will get couples of pictures, the more accurate will be the results doing the average of all the images.

We can thus clearly understand that taking simple pictures of the fluid does not have sense in order to get its displacement, that is why this technique requires two conditions : the studied fluid has to be inseminated by the way of tracer particles and a laser beam is needed to illuminate those particles when the photos are snapped. We will develop in a first part the procedures for the measurement (all the devices and tools used for a PIV experiment), in a second part the settings for our measures (interaction with CFD and the two types of measure realized) and then in a third part the analyze and the results that have been computed.

## **7.3 Procedure for measurement**

### **7.3.1 The security**

Before starting, let's describe an important point for the PIV measurement in regards to the security. As it has been said in the presentation, the PIV technique needs a very powerful laser that the operator has to take into account. The physical security and in particular the eyes protection are compulsory. The laser has a range of power level which can be regulated. The lowest level allows the operator to adjust the laser sheet position, focalize it and the set the orientation (vertical or horizontal) without using protecting goggles but without crossing with any part of his/her body with the light sheet (in fact, the laser remains dangerous for skin and mostly eyes even at the lowest power). The maximum is used for measuring operations and has to be used with goggles which stops the 532 Nm (green light) wavelength that produce the laser which can damage the retina.

Then during the measures at highest level of power, the user(s) has(have) to :

- wear goggles which stops the green light at high power operations ;
- never look straight in the beam ;
- reduce power for alignment operations ;
- avoid beam reflections (isolating the measurement device for example) ;
- the control operations has to be done far enough from the laser ;
- warn others employees when using thanks to a blinking light ;

- work within a closed environment to avoid employees passage.



Figure 12: Laser radiation.

The control of the laser can be done directly from the control unit of the laser or from a PC thanks to cable connections (Serial port and BNC cables). For the setting up, we carefully used the first configuration and for the measurement the second one.

### 7.3.2 The laser

As we described it briefly in the introduction, the laser is a light sheet placed according to the desired plane for which the velocity field wants to be known. For example, if the user wants to compute the velocity field which get out of an air pipe, the PIV can be done transversely (laser sheet perpendicular to the air flow to see orthogonal vortexes) or longitudinally (laser sheet parallel to the flow to see longitudinal vortexes).

Its aim is to illuminate the particles (described below) in order to create a reflection that can be snapped by the camera's objective. This illumination has to occur at least twice within a short time interval. The main advantage of the laser for PIV experiment is its capacity to produce a high energy density monochromatic light.

Many type lasers can be used, they are characterized by the way that the laser light is produced and the emitted wave length of the light. The laser used and directly available in the laboratory for our experiment was of the so-called category : Nd:YAG laser. Without developing too much, we can briefly say that it generates a strong wave length light ( $\lambda=1064$  Nm and  $\lambda=532$  Nm after separation), has the advantage to emit pulse at high frequency and many successive laser pulses can be obtained within a short time.

Laser class	Max output [mJ]	Pulse duration [ns]	Wavelengths [Nm]	Laser medium
4	200	5	1064/532	Nd:YAG

Table 2: Main characteristics of the laser.

### 7.3.3 The inseeded particles

As we said, the measure has to be done by the way of tracer particles which have to follow as best as possible the motion of the fluid and have to be homogeneously distributed. Those particles can be of different nature : smoke, gas, solid or liquid. Below, we summarized a table with the characteristics of many seeding particles used for the PIV for the study of a gas flow :

Type	Material	Mean diameter in $\mu$ m
Solid	Polystyrene	0.5-10
	Alumina $Al_2O_3$	0.2-5
	Polystyrene	0.5-10
	Titania $TiO_2$	0.1-5
	Glass micro-spheres	0.2-3
	Glass micro-balloons	30-100
	Granules for synthetic coatings	10-50
	Dioctylphthalate	1-10
	Smoke	<1
	Liquid	Different oils
Di-ethyl-hexylsebacate (DEHS)		0.5-1.5
Helium-filled soap bubbles		1000-3000

Table 3: Seeding materials for gas flows.

In our case, we chose to use a mixture of glycerin and demineralized water (50%-50%). The seeding particles were generated thanks to Laskin Nozzles described below (we used up to three according to the desired quantity of inseeded particles).

This step needs some notions about the particle's behavior. The sensible point of those particles is that they have to follow as much as possible the motion of the fluid without disturbing it to get accurate results for the PIV. Indeed, the inseeded particles will have a certain inertia and viscosity which must not influence the mean flow. Obviously, having a perfect matching of the particle with the fluid is impossible. Then, a control of the size of the particles has to be done. We will explain it through equations applied to a particle subjected to an acceleration or deceleration.

Before starting, here are listed the different variables used for the following equations :

- $d_p$ : seeding particle diameter [m];
- $\rho_p$ : density of seeding particles [ $\text{kg.m}^{-3}$ ];
- $\rho$ : density of the studied fluid [ $\text{kg.m}^{-3}$ ];
- $\nu$ : cinematic viscosity of the seeder [ $\text{m}^2.\text{s}^{-1}$ ];
- $U$ : velocity of the fluid [ $\text{m.s}^{-1}$ ];
- $U_p$ : velocity of the particles [ $\text{m.s}^{-1}$ ];
- $U_g$ : gravitational induced velocity [ $\text{m.s}^{-1}$ ];
- $U_s$ : velocity lag of a particle [ $\text{m.s}^{-1}$ ];
- $\tau_p$ : relaxation time of the particle [ $\text{s}^{-1}$ ];
- $\tau_f$ : relaxation time of the fluid [ $\text{s}^{-1}$ ]

Let's start from the Stokes' drag law which represent the force generated by the velocity difference between fluid and particle :

$$F_D = 3\pi\mu d(U - U_p) \quad (6)$$

Equation 6 from which it can be deduced the gravitational induced velocity :

$$U_g = d_p^2 \frac{\rho_p - \rho}{18\mu} g \quad (7)$$

An important velocity to define is the one of the particle, which is given by :

$$U_p = U \left[ 1 - \exp\left(\frac{-t}{\tau_p}\right) \right] \quad (8)$$

Then we define the relaxation time of the particle which will be useful to quantify the time of response of a particle submitted to an acceleration or deceleration :

$$\tau_p = d_p^2 \frac{\rho_p}{18\mu} \quad (9)$$

Stokes set up a dimensionless number which compare the relaxation time of a particle respect to the one of the fluid :

$$St = \frac{\tau_p}{\tau_f} \quad (10)$$

The smaller is the relaxation time of the tracer particle respect to the fluid, the better it will follow the velocity flow variation (to reduce it, we can reduce the diameter particle or use a lower density tracer fluid) :

- $St \ll 1$  : ideal tracer ;
- $St < 1$  : acceptable tracer ;
- $St \approx 1$  : “filtered” result ;
- $St > 1$  : modification of the fluid.

The graph of the Figure 13 below shows the time of response of a particle under acceleration in function of its diameter. It can be clearly seen that the smaller is the particle, the more it will follow the motion of the fluid with a limited lag.

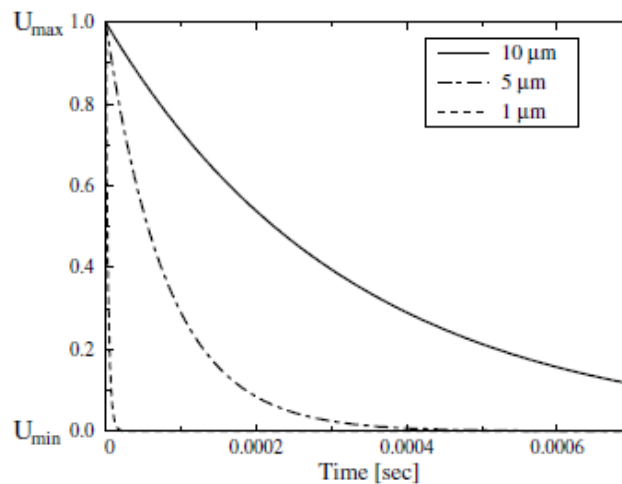


Figure 13: Time of response of a particle under deceleration in function of its diameter.

However a compromise has to be found regarding the size of the particles. They have to be small enough to follow the fluid but not too much so that they can reflect enough intensity to be captured by the camera.

In fact, according to the Mie Scattering theory, it is said that larger is the diameter of the particle, more important will be the light scattered by each single particle. The quality of the PIV recording will depend a lot on it as the quality of the results is sensible to the light. Moreover, the size of the particle has to be larger than the wave length of the laser incident light to apply the previously mentioned theory.

Thus, when the light sheet will meet the particles, a scattered light will reflect in all directions of the space. Below, some diagrams (Figure 14) representing the polar distribution of the intensity

reflected by the particles :

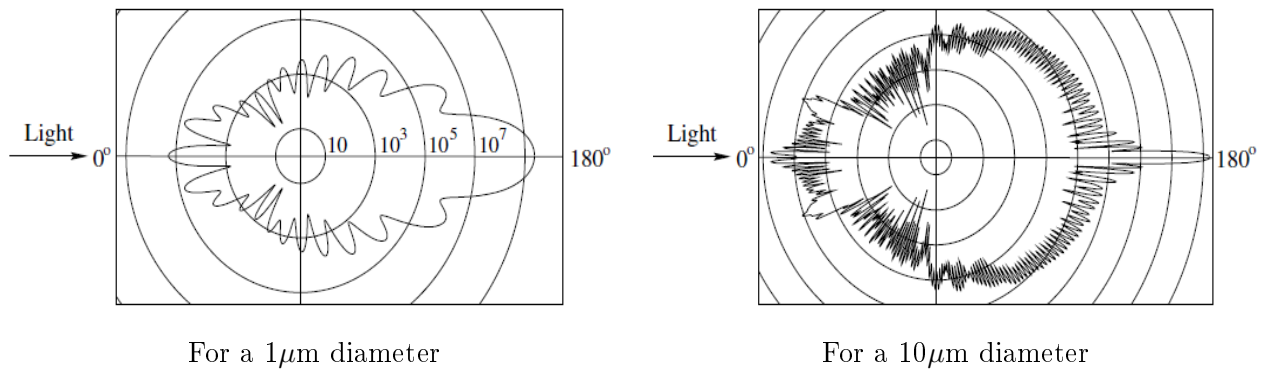


Figure 14: Light scattered by an oil particle in an air flow. The scales are the same.

We can clearly deduce of these diagrams that the ideal angle to record the images would be at  $0^\circ$  and mostly at  $180^\circ$  respect to the incident light. However, a  $0^\circ$  or  $180^\circ$  measurements would not be possible for two reasons: the first is technical and the second is practical. Technical because we want to practice a 3D stereoscopic PIV and thus we need to use two cameras positioned with a certain angle with respect to the axis of the flow and to the measurement plane. And then practical because if the camera is placed in front of the flow, the oily particles present in the arriving flow would dirty the objective and thus distort the measurement.

In our experiments, we choose to use glycerin (in water) droplets seeding because of their non-toxicity (no need to use treatment system for the outgoing inseeded air) and also because of a relatively homogeneity of the particle size. The seeding particle generation is created thanks to Laskin Nozzles (see Figure 15). The principle of this technique is that four pipes dive into a tank filled with the seeding oil. Pressurized air is sent through those pipes and get out thanks to tiny holes. This creates a vaporization of the oil which is sent to the outlet pipe toward the experiment. The quantity of the inseeded particles can be controlled alimenting with pressurized air one, two, three or the four pipes. Moreover the particle concentration can be controlled thanks to another pressure inlet which set a certain pressure into the tank.

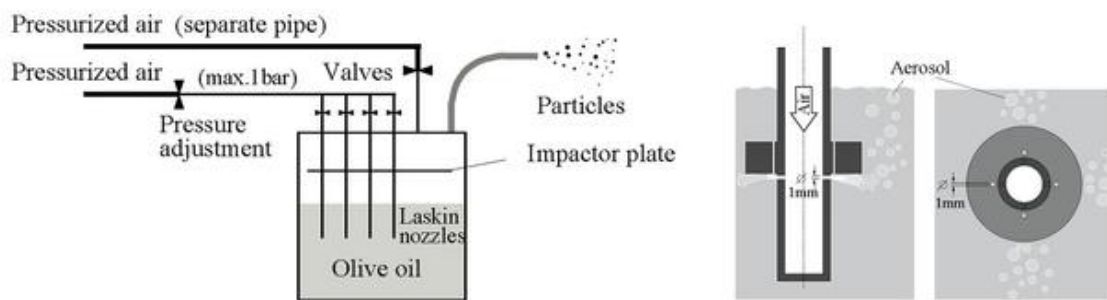


Figure 15: Principle of a Laskin Nozzle.

### 7.3.4 The cameras

For a 2D PIV, one single camera is necessary as we just want to get two velocity components ( $x$  and  $y$ ). However for a 3D, we want to get the third component ( $z$ ). This velocity field is represented on maps which will be shown later.

To do it we use two cameras. The principle is simple and based on the human's eye principle (see Figure 16 below) : it consists in seeing something with the same angle shift respect to a median line in order to recreate the deep coordinate ( $z$ ).

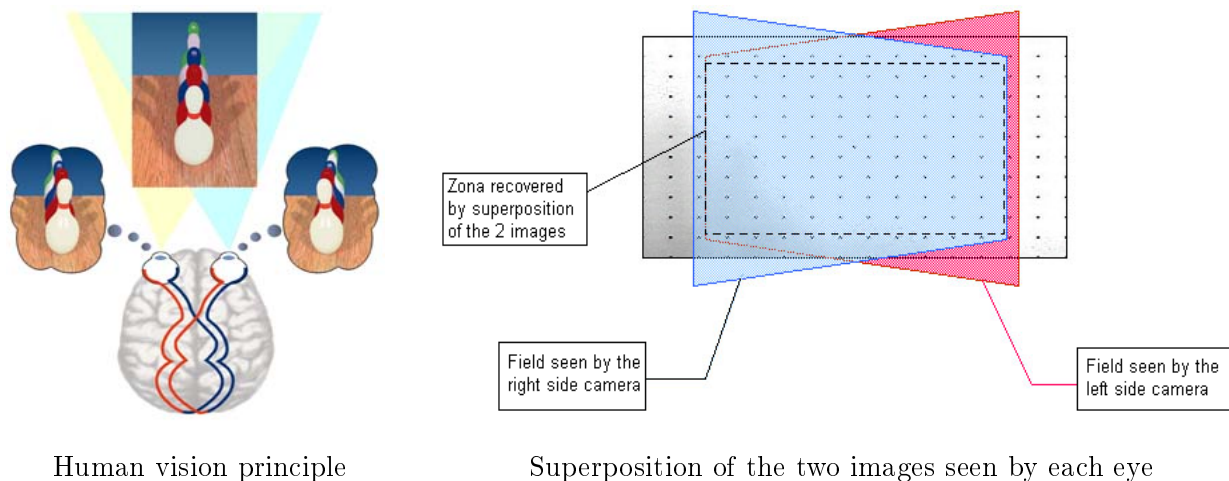


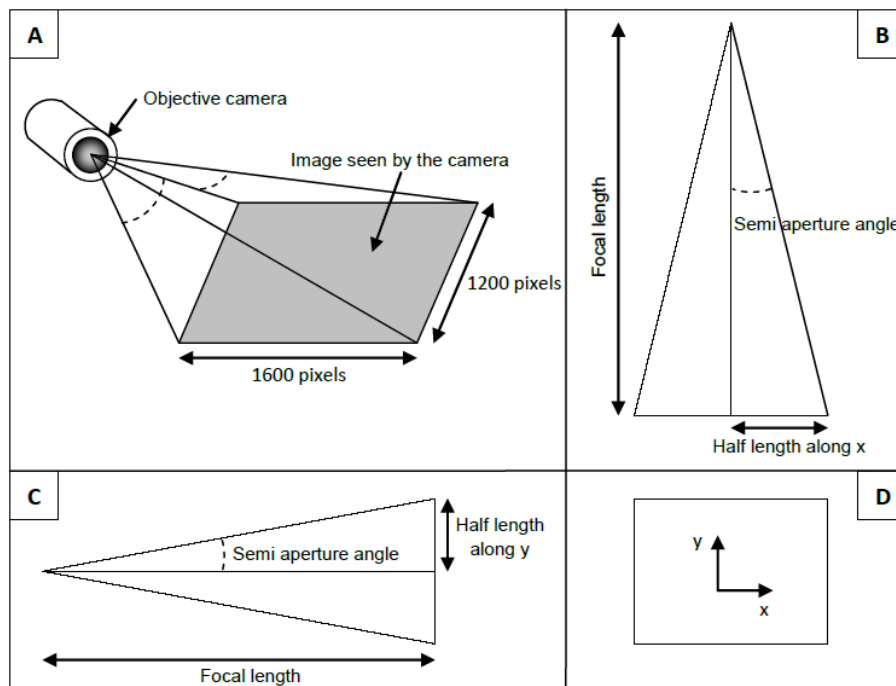
Figure 16: Similitude human vision with PIV 3D.

Each eye sees a different image and the brain is able to construct a single image which takes into account the depth.

The cameras are constituted by a sensor and an objective. The sensor has the goal to discretize the continuous image the eye can see. The most powerful the sensor is, the more information the user can get (example of the commercial digital cameras with pictures resolution of 10, 12 or even 14

Megapixels). The sensor captures the image in term of pixels. The sensors we used for our experiments were 1600x1200 pixels (around 2 Megapixels) and of the family of the CCD cameras. The main advantage of these CCD sensor is that they can scatter two pictures in raw within an extremely short time (with the order of the microsecond).

The second essential component of the camera is the objective. According to its cone angle (see figure 17), we can play on the distance camera/plane of measurement. The objectives we used for our experimentations were not able to zoom, thus to zoom in on something, we had to move closer the camera and vice versa to zoom out.



A : Angles of aperture of the objective. B : Vision's angle of the camera along x.  
 C : Vision's angle of the camera along y. D : Image seen by the camera (ratio 4:3).

Figure 17: Image seen by the camera and aperture angles.

In fact, in some cases, the camera can be close to the measurement plane but in some others, for example if the measurement plane is in a high velocity zone, we cannot risk to damage the device thus the camera have to be far enough from the device. For our two PIV experiments, we used two different objectives according to the type of measure we did. Below, the Table 4 which sum up the main optic characteristics of those linked to the drawings of the Figure 17 :

	Focal length [mm]	Half length along X axis [mm]	Aperture angle along X axis [°]	Half length along Y axis [mm]	Aperture angle along Y axis [°]
Objective 1	24	5.92	27.71	4.44	20.96
Objective 2	60	5.92	11.27	4.44	8.46

Table 4: Main features of the two used objectives.

The half lengths of the images seen by the objectives are computed thanks to the scale meter/pixel ( $7.40\mu\text{m}/\text{pixel}$ ) considering that the sensor has a 1600x1200 resolution. Thanks to these half lengths, the focal lengths and trigonometric laws (see Figure 17), we can compute the semi-angles of aperture (and then the full angle of aperture) of the objective along X and Y axis.

We will see further in which case we use one or the other. Now let's introduce another part of the job linked to the camera, which is the focusing and calibration for the measurement.

### 7.3.5 Focusing and calibration

The quality of the results will depend a lot on these two steps which consist in focusing perfectly the image (to see one inseminated particle as a bright point light and not as a blurred light) and calibrate the two cameras (in preparation for overlaying the images and recreate the third coordinate for the maps).

The focusing:

During the step of the calibration the focusing has to be done very precisely. To have the best results of calibration we need very neat images with the best resolution. For that step, it has been done with the diaphragm totally opened and just the ambient light.

The calibration:

The two cameras used for the stereoscopic PIV have to be placed with the same inclination (we need to see the same view from the two different cameras.) with respect to the plan that we want to measure; it is the angle that gives the third dimension.

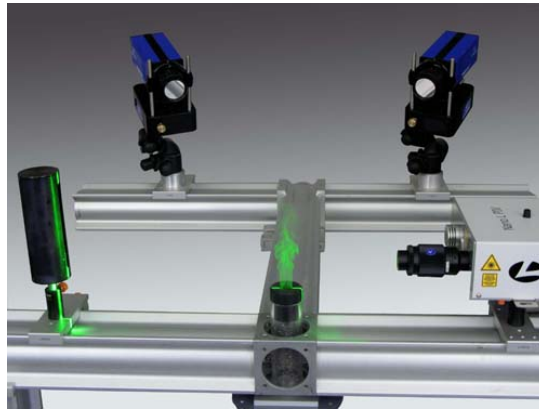
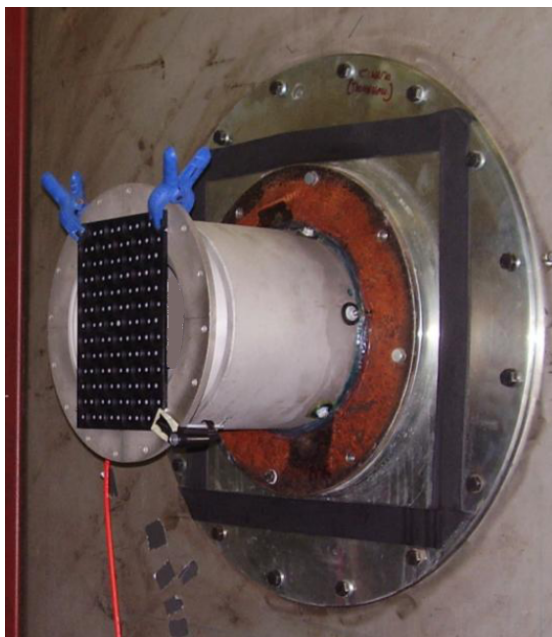
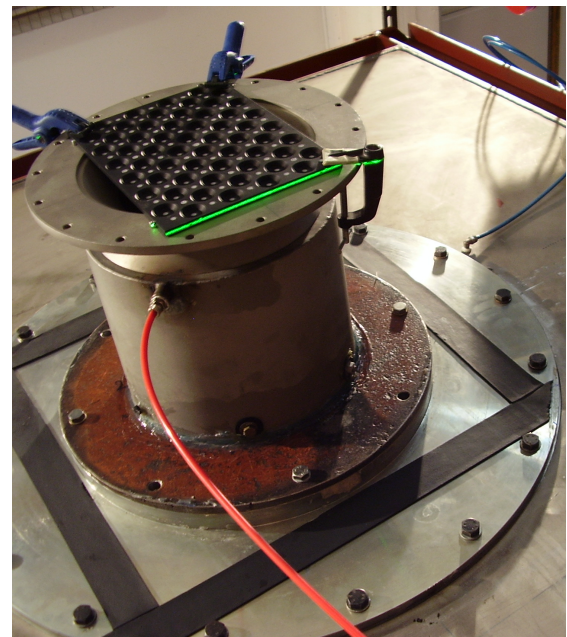


Figure 18: The two cameras with an inclination angle respect to the measurement plane.

This is a very important part of the setting; indeed the software will join and bound the information of the calibration thanks to what have been measured during the flow test. The calibration is done thanks to a target (see Figure 19) fixed at the place in which the user wants to do the measurement. With the calibration, the software will be able to get close velocity with the spacing between images taken by each camera. The software will reconstruct the third dimension (to have finally a 3D representation of the velocity field) as our eyes and brain do (see Figure 16). This experimentation needs a lot of precautions from the users. In fact the installation is very delicate and if the camera is moved (even a little bit), the calibration has to be redone.



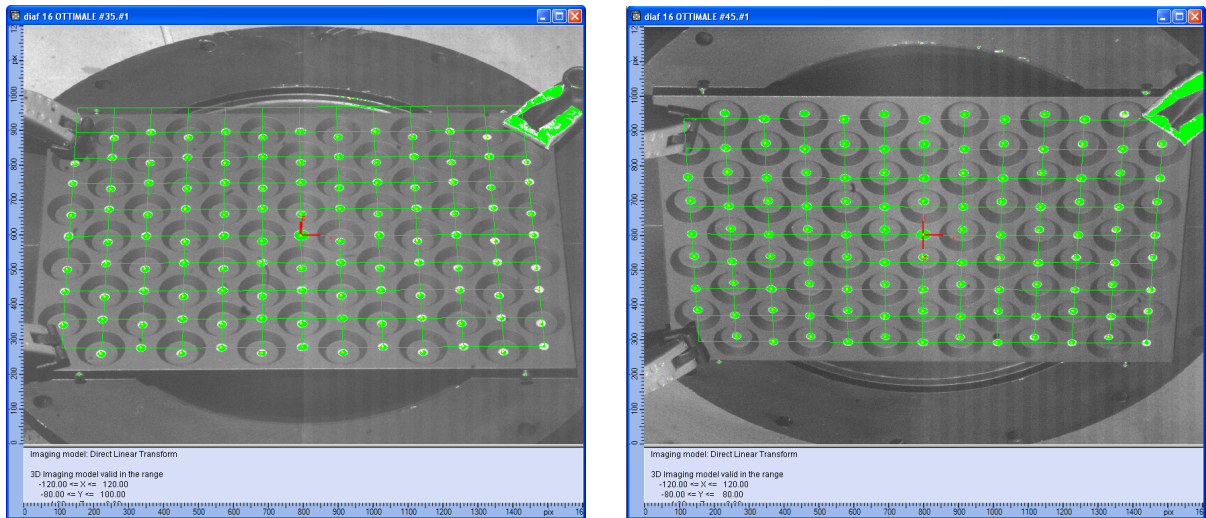
Target set



Laser seen hitting the target from below

Figure 19: Target set at the place of the measurement plane.

The target is a black plate with equally spaced white dots (in order to create a huge contrast) and a certain relief (in order to understand the third component). But to amplify this contrast between black and white, it has been used a powerful lamp to illuminate the target in the dark to make the dots more bright. The diaphragm of the cameras was opened at the minimum aperture (f/1.8) in sort of having the best reception of the deepness and protect the objective. For the calibration, each camera takes one picture of the target. And then, thanks to an algorithm, a grid is generated by the software for each image and the perspective will be created by combination of these two grids and based upon the central dot of the target :



Calibration grid seen by the camera 1

Calibration grid seen by the camera 2

Figure 20: Calibration grids generated by the software.

The perfect symmetry of the images seen by the cameras (Figure 20) is required to reconstruct the 3D plan if we want to have to good representation of the flow motion. Moreover, this step is delicate because very sensible to the focusing of the cameras on the measurement plane.

## 7.4 Setting up the PIV experiment

### 7.4.1 Coherence of the experiment with the CFD

As it has been explained in the part “Context and goal of the internship” this PIV experiment has the goal to study a swirler. This component was decided to be studied through a numerical (CFD), an experimental analysis (this PIV experiment) and then to confront them. Obviously, to be compared, the physical conditions have to be the same. Then, starting from the numerical analysis (done previously by our colleagues taking into account the combustion, that is to say in hot conditions)

three air flow rates according to different theories has been defined and chosen to be imposed to set the PIV operating conditions. The theories considered are:

- the similitude of Euler ;
- the similitude of Reynolds ;
- the conservation of the volumetric flow rate.

It has been chosen to study different cases because, to be able to confront theory and experimental, many different parameters can be fixed which will be explained for each case. We are now going to explain each single similitude criterion.

Firstly, let's define some variables :

- $v_1$ ,  $T_1$ ,  $P_1$ ,  $\rho_1$  and  $\mu_1$  respectively mean values of velocity, temperature, pressure, density and cinematic viscosity in CFD conditions for the study of a flame in an intermediate section of the combustion chamber ;
- $v_2$ ,  $T_2$ ,  $P_2$ ,  $\rho_2$  and  $\mu_2$  respectively velocity, temperature, pressure, density and cinematic viscosity in our laboratory conditions, that is to say at cold conditions ;
- $\Delta P$  the pressure difference between upstream and downstream of the component = pressure drop ;
- $A$  ( $= A_1 = A_2$ ) the section of the flame tube considered as constant.

#### 1 - The similitude of Euler :

This similitude is mainly used for turbine problems. It can be applied for the case in which we want to maintain constant the pressure drop between cold and hot case. We define the Euler number as :

$$Eu = \frac{v}{\sqrt{\frac{2\Delta P}{\rho}}} \quad (11)$$

Then we consider the conservation of the Euler number :

$$Eu_1 = Eu_2 \quad (12)$$

Then considering the gas perfect law ( $P=\rho rT$ ), we can deduce that :

$$\frac{v_1}{v_2} = \sqrt{\frac{T_1}{T_2}} \quad (13)$$

Then, we take into account the conservation of the mass flow rate in both cases  $\dot{m}=\rho vA$  and we substitute into (13) :

$$\dot{m}_2 = \dot{m}_1 \frac{\rho_2}{\rho_1} \sqrt{\frac{T_2}{T_1}} \quad (14)$$

Finally, it has been found that to maintain the drop pressure constant between hot and cold cases, the mass flow rate have to fixed to :

$$\dot{m}_2 = 1.012 \text{ kg.s}^{-1} \quad (15)$$

### 2 - The similitude of Reynolds :

Let's define the Reynolds number :

$$Re = \frac{\rho v d}{\mu} \quad (16)$$

And we want to fix the Reynolds number :

$$Re_1 = Re_2 \quad (17)$$

Then, we take into account the conservation of the mass flow rate in both cases  $\dot{m}=\rho vA$  and we substitute into (17) :

$$\dot{m}_2 = \dot{m}_1 \frac{\mu_2}{\mu_1} \quad (18)$$

Finally, it has been found that to maintain the Reynolds number constant between hot and cold cases, the mass flow rate have to fixed to :

$$\dot{m}_2 \approx 9 \text{ kg.s}^{-1} \quad (19)$$

### 3 - The volumetric flow rate conservation :

In that third case, it has been decided to maintain to volumetric flow rate or velocity :

$$\frac{\dot{m}_1}{\rho_1 A_1} = \frac{\dot{m}_2}{\rho_2 A_2} \quad (20)$$

Considering that  $A_1 = A_2$  and isolating  $\dot{m}$ , we get the mass flow rate to fix if we want to maintain the velocity constant in both cases :

$$\dot{m}_2 = \dot{m}_1 \frac{\rho_2}{\rho_1} \quad (21)$$

Then finally, it has been found :

$$\dot{m}_2 = 1.442 \text{ kg.s}^{-1} \quad (22)$$

Then to sum up, we found these three mass flow rates to respect for our PIV experiments :

Similitude	Euler	Reynolds	Velocity
Portata [kg.s <sup>-1</sup> ]	1.012	9	1.442

Table 5: Mass flow rates to fix to have similitude CFD/PIV experiment.

Regarding to the flow rate obtained for the Reynolds case, it was physically impossible in the laboratory to reach such a value because of the limited capacity of the ventilator, with the specific configuration of the experiment, then for that similitude, it has been decided to do it with the maximum that the fan could reach ( $\approx 1.62 \text{ kg.s}^{-1}$ ).

Moreover, our PIV experiment had certain strains : in fact, the swirler was set with a certain orientation and was maintained on the flange by the way of a fixation rod which could create non uniformity of the flow. Then the numerical computation has been redone to correspond exactly to the same operative conditions that is to say in “cold” conditions and with the geometry of the swirler as it was mounted in our case.

#### 7.4.2 The devices and planes of measurement

In this section, we will explain the very precise and tough job of setting up the PIV experimentation. In fact, the quality of the results will depend a lot on the quality and care of the installation of all the devices described previously and listed below. The user has to be very careful and pay a lot of attention when he places everything.

The material we used for our stereoscopic PIV measurements :

- 2 sensors CCD 1600x1200 pixels ;
- 2 objectives (24 mm or 60 mm according to the desired measure) ;
- 1 target to calibrate the system in order to take into account the third dimension ;
- 1 laser Nd:YAG - 1064 nm - 532 nm ;
- 1 mirror to reflect the laser beam in the desired direction ;

- 1 bench to carry the laser and the mirror ;
- 2 tripods for both cameras ;

The first step is to choose the desired plane measurement. For the studied swirler, it has been decided by the engineering team to compute the transverse and then longitudinal plane in order to see how reacts the component and how the vortexes develop under different flow rates.

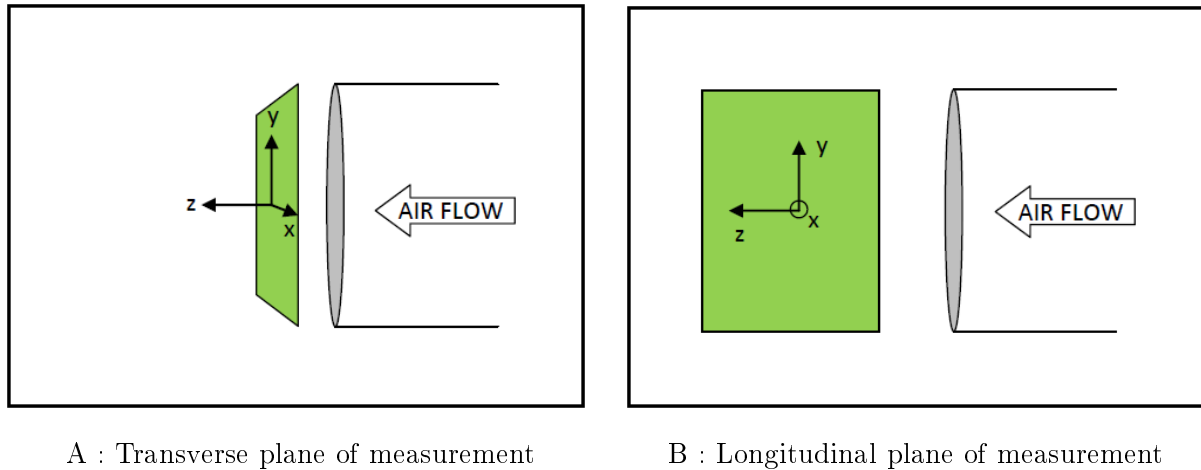


Figure 21: The two different planes of measurement chosen for the PIV.

All the setting up of the measurement line **MUST BE** done very precisely. The quality, accuracy and reliability of the results depend on it. Now, we will develop the procedure we followed to set up both measures, the main difference is on the layout and orientation of the cameras and the laser sheet.

The component to test was a burner constituted by many fuel nozzles (mounted in slots) and a swirler to create the mix air/fuel. It was mounted on a flange and connected upstream to the air plenum defined previously (Figure 8 and Figure 22 below). We just focused on the role of the swirler and so tested a simplified component, so without considering the nozzles (slots were empty). The goal is to see the structures of the momentum quantity created by the swirler in order to have a flow field to be compared with the CFD calculation, simplified in the same way.

A distinction between the two measurements is that downstream in one case the component was let free and blew the air directly into the lab (transverse plane of measurement) and in the other case the flow was confined into a liner before expelling the air out (longitudinal plane of measurement). For the longitudinal test, the component was followed by 3 distinct cylinders (in correspondence with the Figure 22 below) :

- A : a dummy liner : its goal is to channel flow and it ends with a Venturi to create an acceleration of the fluid ;
- B : the test section liner : fitted out with 4 Plexiglas windows, two, symmetrical, will serve to let the light sheet go through the section test (the light enters and goes out to avoid laser reflexion which would disturb the measure) and the two others, also symmetrical, will serve to visualize the flow thanks to the 2 cameras ;
- C : the final liner : to eject the flow.

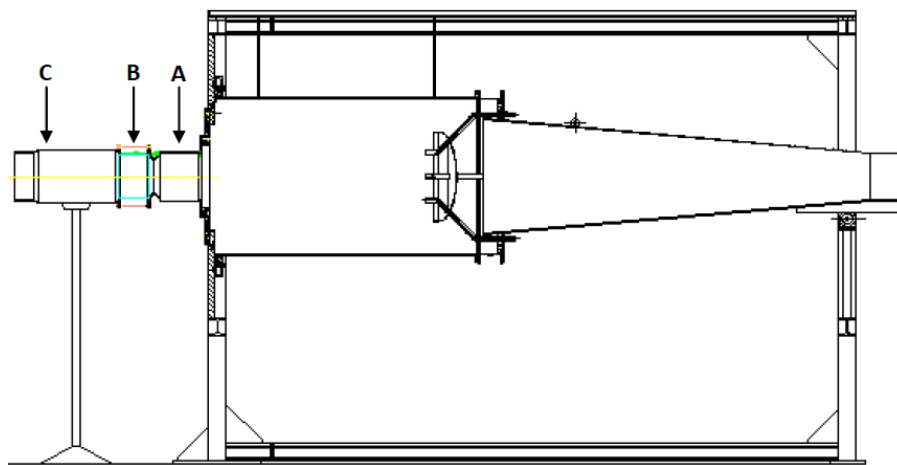
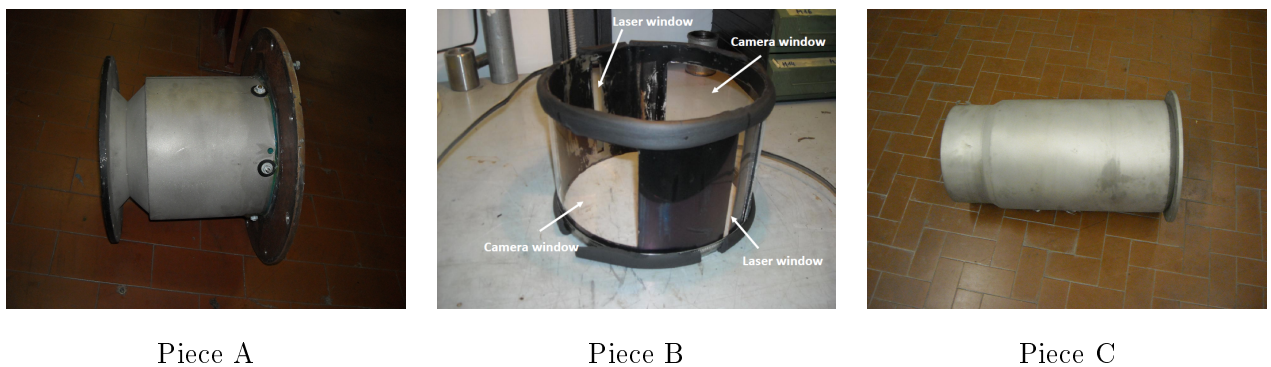


Figure 22: Measurement line for PIV experiment.

The solution of the confined flow has been chosen because it represents as best as possible the reality of the flame tube into the combustion chamber. Configuration which was not possible for the transverse plane because of the complexity of the liner (the part B) which should have been realized to let the laser comes in and the cameras watch in. Transverse measurement has been done only with the part A. We detailed here each pieces A, B, and C :



Piece A

Piece B

Piece C

Figure 23: Constitutive pieces of the liner.

### 7.4.3 Transverse section measurement

The first measurement we choose to do was orthogonal to the flow. Then the first thing we did was to align the laser with the first available surface in order to have the flow field less affected by the not confinement. That is to say immediately after the first outlet flange. This has been done thanks to the mirror and it has to be perfectly leaned in order to straighten up vertically the laser sheet at  $90^\circ$  precisely and correspond to the desired transverse plane measurement (picture A on Figure 21 and Figure 24 below) :

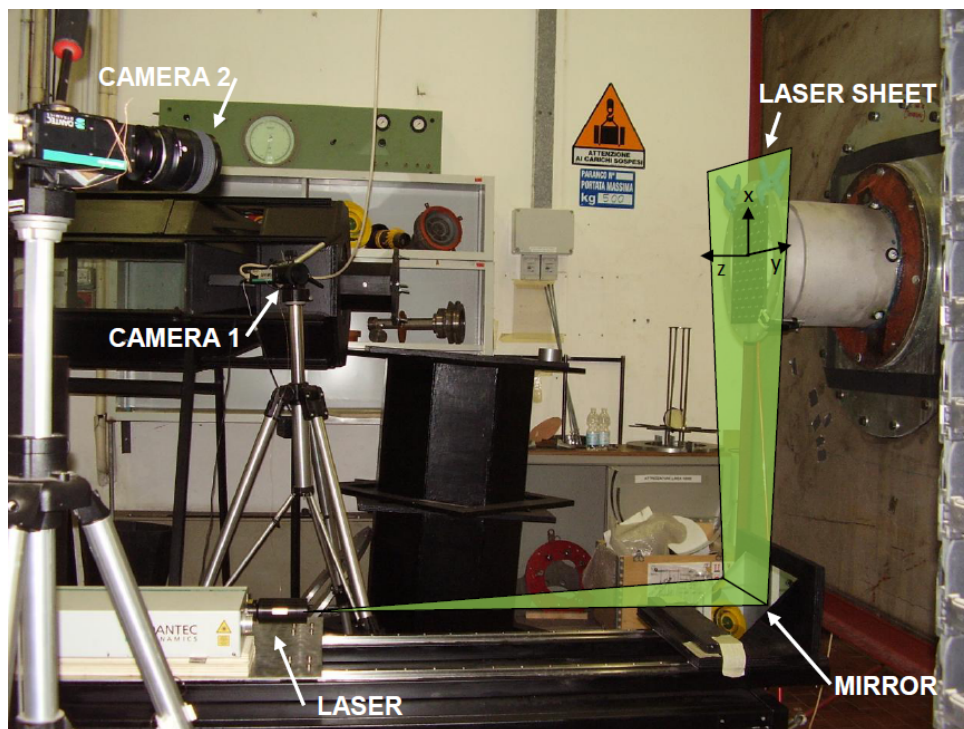


Figure 24: Layout for the transverse PIV.

Then the target is placed in correspondence of the plane of measurement and maintained by the way of grips (Figure 25 below). The center of it has to match perfectly with the center of the tested component and also to be perfectly horizontally in order to create the calibration of the system (thus the software generates a grid so that it could take into account the third component of the velocity as it has been developed in the part “Calibration and focusing”).

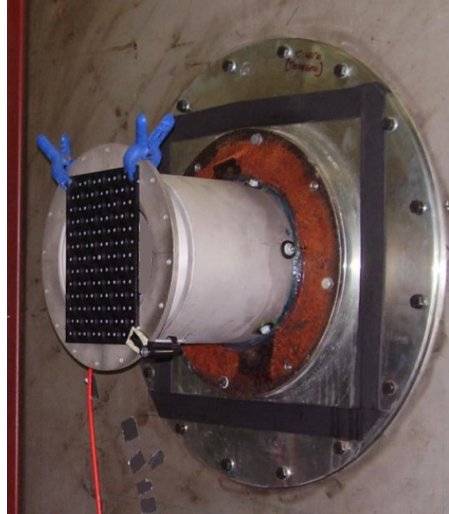


Figure 25: Target ready for calibration at the place of the measurement plane.

For the transverse section measurement, the 60 mm objective has been used because of its small aperture angle. In fact, as the flow was not confined the cameras had to be placed far enough from the outlet of the device (see Table 4). Then we placed both symmetrically and at  $30^\circ$  respect to the flow axis the cameras mounted on their tripod (thus each camera will see the outlet with a certain perspective and the combination of these two perspectives will reconstruct the depth of the motion field). The image of the measurement plane has to cover the whole diameter of the outlet section thus the cameras have to be placed sufficiently far away from the outlet so that the optic cone intercept the diameter of the outlet (see the Table 4 with the characteristics of the objectives and their aperture angles).

Then we have rotated both cameras of  $90^\circ$  in order to see a  $1200 \times 1600$  pixels plane instead of  $1600 \times 1200$  pixels. Thereby, the prospective image will exploit as best as possible the measurement plane and what happened vertically on the whole diameter (in fact, in both configurations, the laser will flash vertically). In fact, both cameras, set in this way, have a trapezoidal vision. The interception of both images in the software will create a common oval zone. The optic laws explain that rotating the cameras at  $90^\circ$  will give the biggest size for this zone :

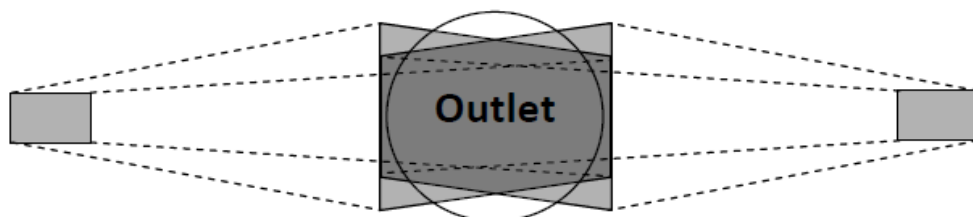


Figure 26: Horizontal perspective seen by the crossed zone of the two cameras.

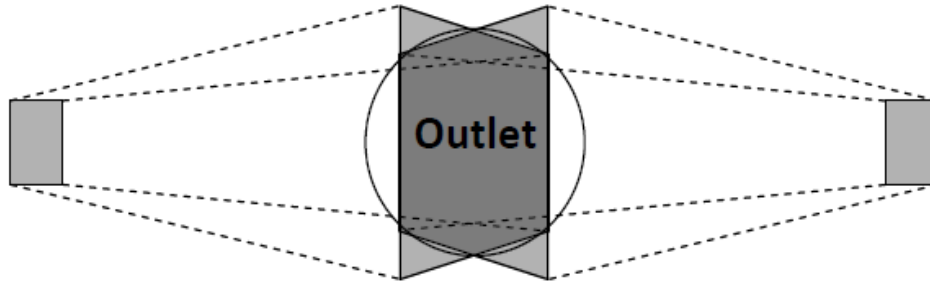


Figure 27: Vertical perspective seen by the crossed zone of the two cameras.

So we can clearly see that the seen zone will be bigger rotating the cameras and will exploit the whole diameter of the outlet. This logic will be also valid for the longitudinal plane of measurement.

Then, once the cameras are placed, we check on the DynamicStudio software that the center of the image seen by both cameras corresponds exactly to the center of the target and thus that both images are symmetrically identical (as seen on the Figure 20).

Then comes the most delicate part, the one in which we have to calibrate the software in order to compute the 3D as explained in the part “Focusing and calibration”.

Let’s now explain the configuration and setting up of the longitudinal plane.

#### 7.4.4 Longitudinal section measurement

The longitudinal measurement compare to the transverse has been done, as we said, through a cylinder (diameter = 237.5 mm and length = 170 mm) with transparent windows in order to have a confined flow (see the representation on the Figure 28 below). The sizing of these windows have not been chosen randomly and will be described below.

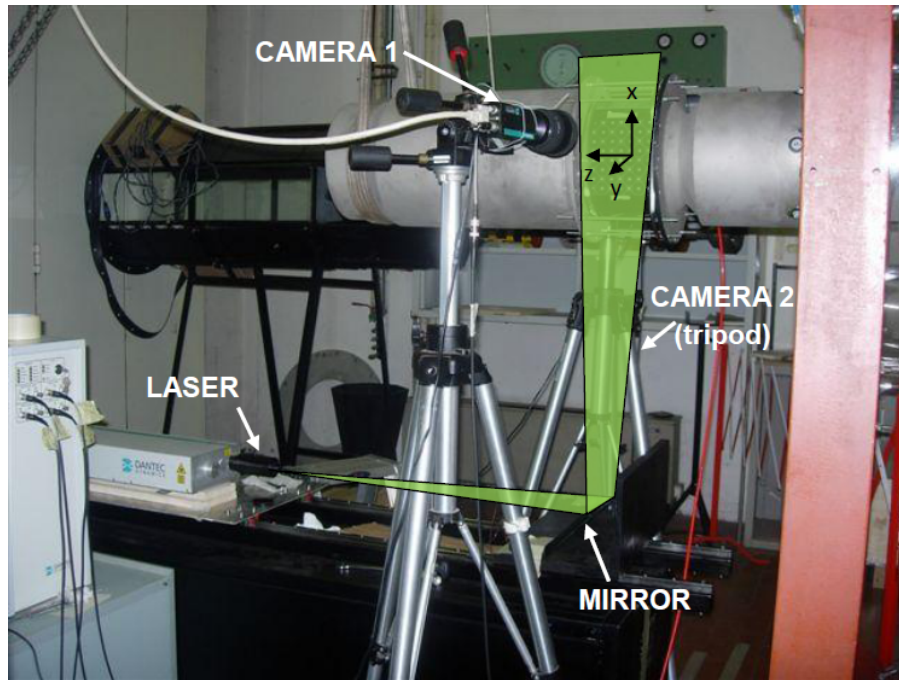
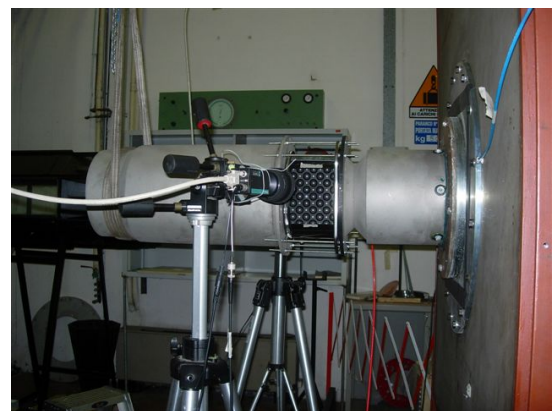
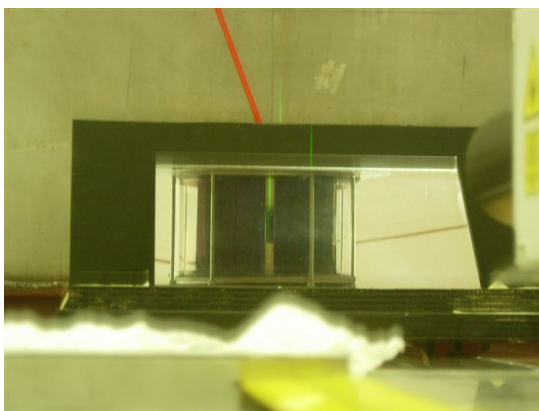


Figure 28: Layout for the longitudinal PIV.

Then, the light sheet has been set perfectly vertical (thanks to the mirror and rotating the lens of the laser) in the same way than previously (Picture A on Figure 29) and the target maintained inside the cylinder, positioned in correspondence to the longitudinal measurement plane to be seen by both cameras (Picture B on Figure 29). For the longitudinal section measurement, the 24 mm objective has been used because of its larger aperture angle (compare to the one of the 60 mm). In fact, as the flow was confined, the cameras could be placed close to the outlet of the device (see Table 4) and it was also necessary in order to optimize the shot of the resulting image.



A : Laser sheet seen from below through the mirror. B : Target placed in the liner for calibration.

Figure 29: Laser and target set up.

The hardest part of the longitudinal measurement was to align the cameras perfectly with the same angle, in order to see exactly the same image from two opposite points of view and above all through the windows. Let's remind that the cameras are rotated by  $90^\circ$  (Figure 26 and 27).

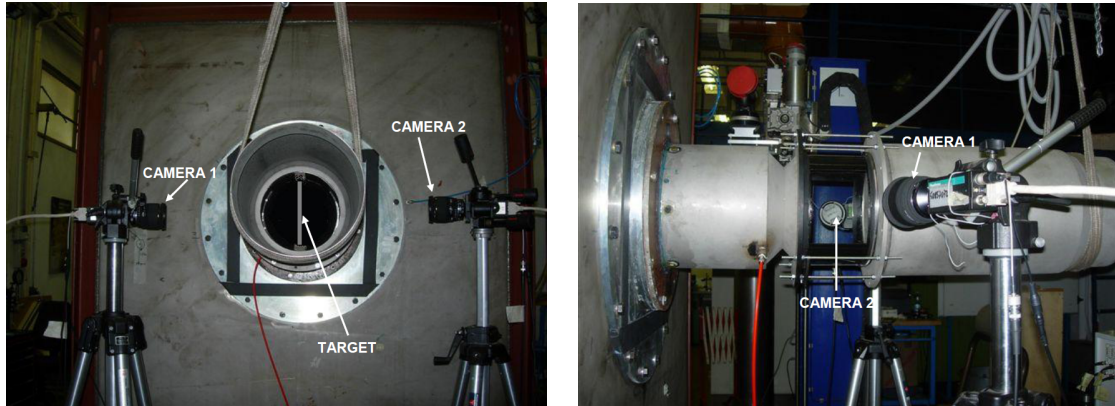


Figure 30: View of the target position and of the overall layout of the cameras (symmetric on the right picture).

Then, the same procedure than for the transverse plane regarding to the calibration and the generation of the grids has been applied.

As we said, the test section is embedded with four windows. As all the components are steel made, to let the light sheet and the cameras to access, Plexiglas pieces window have to be inserted. The size of the two which let the laser comes in and out had to be long and large enough to let the laser flash in (around 10 mm width). However, the size of the two camera windows cannot be chosen randomly. In fact to ensure the mechanical strengths of the set, the size of these windows cannot be too large but also not too tiny in order to visualize, thanks to the cameras, an interception between the light sheet and the flow as large as possible according to the objective size (see characteristics in Table 4 for the 24mm objective).

Thanks to the features of the objective, there are two options on which we can play :

- the distance of the camera respect to the window with a fixed size of window;
- or the size of the window with a fixed distance of the camera (the chosen option).

The strain is that we would like to see the whole inner diameter of the test section (= 237.5 mm). We can clearly deduce, thanks to the sketches below (Figure 31 and 32), that putting closer the camera reduce the dimension of the image seen by the objective and putting it further increase that size (due to the fixed aperture angle on our objectives).

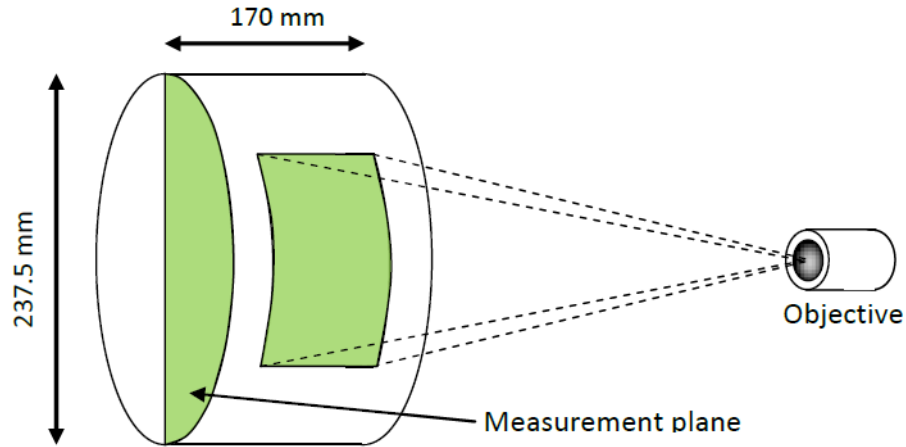


Figure 31: Camera snapping into the test section.

Then we computed the length of the window ( $l_w$ ) according to the following sketch :

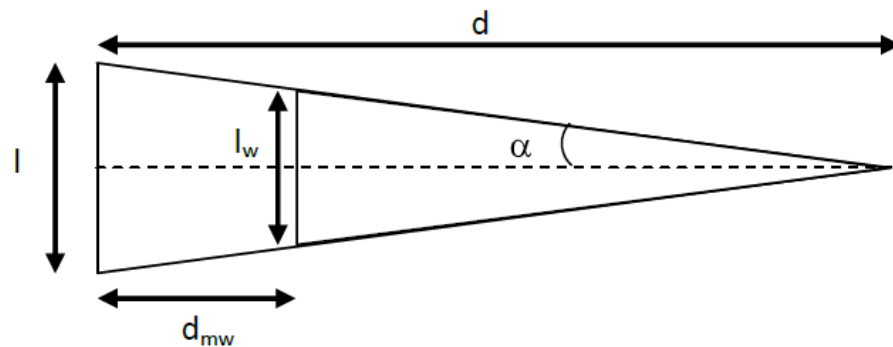


Figure 32: The further the camera is, the largest will be the measurement plane intercepted.

With the following variables :

- $l$  : length of the measurement plane (= diameter of the test section = 237.5 mm);
- $d$  : distance measurement plane - camera;
- $\alpha$  : semi aperture angle for the 24 mm objective (= 13,86°);
- $l_w$  : length of the window;
- $d_{mw}$  : distance measurement plane - window (= half of the test section diameter = 118.75 mm).

Then thanks to the basic trigonometric equations, we calculated  $l_w$  with the camera located at a distance  $d$  :

$$d = \frac{l/2}{\tan \alpha} = 418.42 \text{ mm} \quad (23)$$

$$l_w = 2 * (d - d_{mw}) * \tan \alpha = 178.92 \text{ mm} \quad (24)$$

Then we found the length of the windows. Regarding to the windows' width we choose the biggest as possible to see the longest mixing zone, keeping large enough the edges of the cylinder for the mechanical strength. We used cardboard to recreate the cylinder in which we cut the window and tried to visualize the target inside.

However, we noticed that the calculated effective view was not exactly the one we expected to see on the PC due to the fact that the test section is cylindrical and then curved (not straight as considered for the calculation). Then, we took into account the curvature of the component and used Autocad software in order to get the right dimensions to cut. Finally, the windows have the following dimensions : 168 mm long and 120 mm wide.

Finally, the windows have been cut into the cylinder and it has been completely wrapped with a thin Plexiglas sheet treated anti reflection. The metal part of the cylinder has also been painted in black to avoid any reflections.

#### 7.4.5 Parameters of the software

For the acquisition of the data, the control of the whole system (laser + cameras) is synchronized and done at distance by the operator. From the DynamicStudio panel control, many parameters can be controlled :

- **Time between pulses** : this is the interval of time between the two couples of pictures snapped by one camera. This time obviously is link to the velocity of the studied flow, the faster it will be, the shorter will be this characteristic time. Its unit is in  $\mu s$  and the minimum time that can be computed is  $t = 0.02 \mu s$ . In our different measurements, we chose times from  $8 \mu s$  (for the "slowest" flow rate) to  $4 \mu s$  (for the fastest) ;
- **Trigger rate** : this is the frequency of the laser. At each flash will correspond a couple of images snapped. It is limited by the capacities of the camera. In our case, the frequency range the user can be set within this interval :  $f = [0;15]$  Hz. For our measurements, we used the faster frequency we could set, that is to say 15 Hz ;
- **Number of images** : this is the number of couples of images the user want to acquire. The more there will be, better will be the results for an average processing of the data. It depends a lot of the available RAM memory capacity of the computer (buffer). In our case, we were limited by this and captured around 160 couples of images for each camera and for each measure ;

- **Single/Double frame mode** : the software can specify to the camera to scatter either one image or a couple of images within a short time. For the calibration of the system, the single frame mode is sufficient and for the PIV experiment, a couple of images was necessary.

As we explained in the PIV principle, a couple of images is snapped within very a short moment by each camera and at the same time. However, these pictures cannot be used immediately, they have to pass through an image processing. We will develop later the functions used step by step for post treating these results starting from a basic image. We gave here a representation (Figure 33) of the capturing sequence of the images during the PIV experiment :

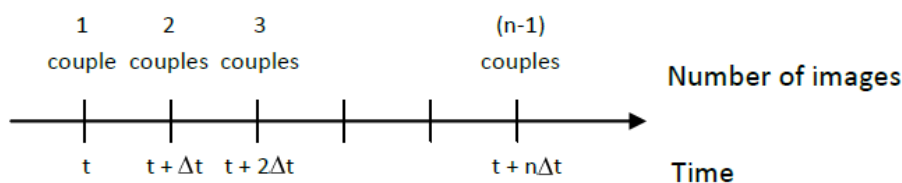


Figure 33: Images capturing sequence for one camera. Note :  $t$  is the starting time of the experiment,  $\Delta t$  correspond to the previously defined “Time between pulses” linked to the flow velocity and  $n$  to the “Number of images” to acquire.

Thus considering the couples of images and the two cameras we start from  $4*(n-1)$  images. Then, after having explained the PIV principle, the tools used for it and the specificity of our measures, we are going to exposed our results.

## 7.5 Analysis and results

### 7.5.1 The test sequences

As it has been explained in the part “Coherence of the experiment with the PIV”, the measurements took place according to three air flow rates :

Physical similitude	Euler	Velocity	Reynolds
Air mass flow rate [kg.s <sup>-1</sup> ]	1.012	1.442	1.62

Table 6: Mass flow rate used in function of the similitude criterion.

We cannot reach the same condition as it has been chosen previously, indeed, it was predicted a air flow rate for the three similitudes as it figures on the table overhead. These air flow rates had been chosen for a temperature of 25 C and a air density of 1,179 kg/m<sup>3</sup>. We want to keep the same conditions, which respect the temperature and air flow imposition. Temperature increases in the air bench as well as we input a major air flow rate.

Taking into account the input condition, we take the conversion with the temperature of the flow and reach the flow rate.

$$\rho_{bench} = \frac{\rho_{input} \times T_{input}}{T_{bench}} \quad (25)$$

$$Q_{bench} = \dot{m}_{input} \times \rho_{bench} \quad (26)$$

If we want to be very accurate, we have to take care of maintaining during the all period of the registration this condition; get closer of the mass flow rate regarding to the air temperature. It guaranties the quality of our results for the comparison with the CFD.

Before picking up the real measures, we made some tests to determine the optimal flow rate of inseeded particles to use for each air mass flow rate in order to have readable results. For this, we used up to three Laskin nozzle atomizers to have a tracer particle density big enough for the highest flow rate.

### 7.5.2 The results and statistical processing

As the post processing is the same and has the same effect for each measure, we will start detailing the step-by-step processing procedure (from the basic image and to the clean readable image) for the case of the transverse measurement for the lower mass flow rate (i.e : 1.012 kg/s). Then, we will present the result as a confront between the transverse and longitudinal measurements for each desired similitude (corresponding to a mass flow rate - see Table 6). For each step, we will explain the principle and the effects of the functions used (act the same way on each image).

After having launch the experiment, we get that kind of picture :

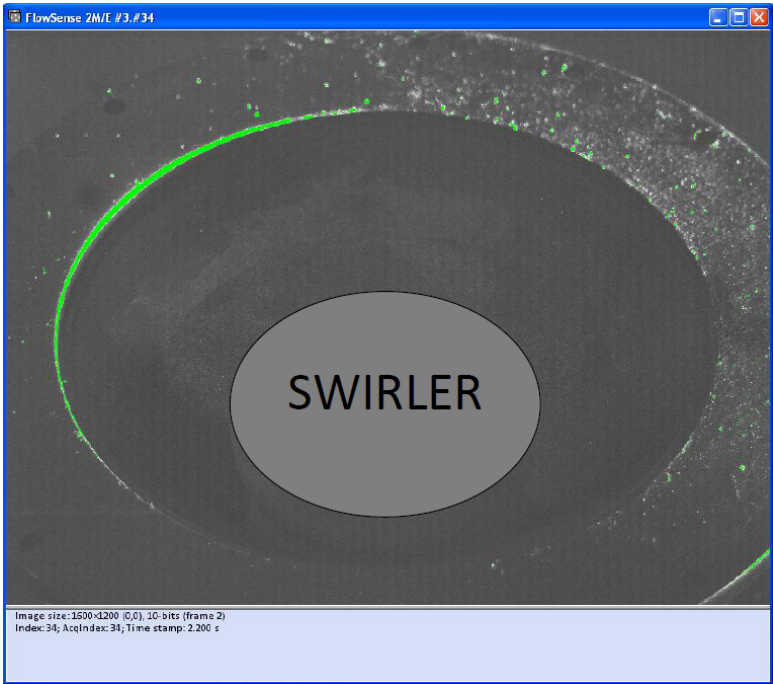


Figure 34: Image captured by the software.

That kind of image is obtained  $4*(n-1)$  times (see Figure 33). Then comes the first image processing (*Image Min/Max*) which keeps and isolates the “fixed” background which is identical for each pictures :

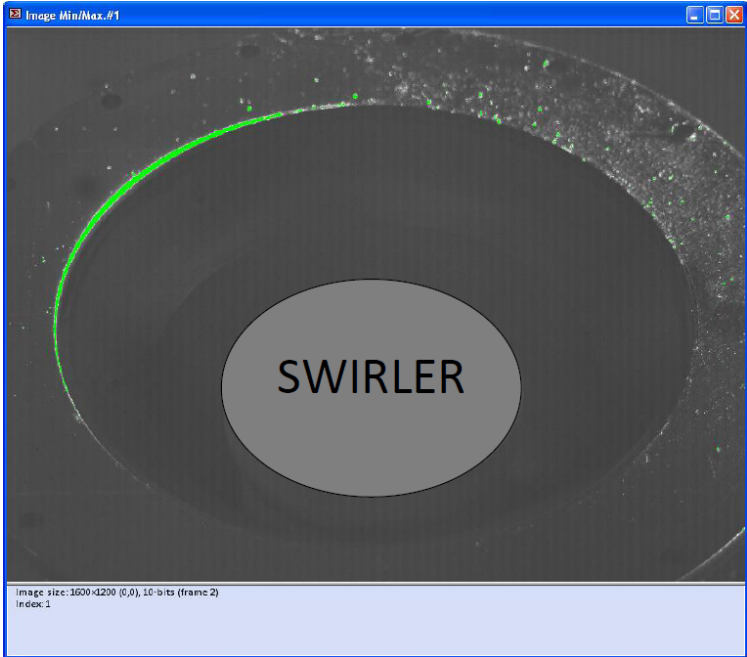


Figure 35: Background isolated.

Then the Figure 35 is subtracted to the Figure 34 in order to keep only the illuminated moving particle (we can distinguish in the center of the image) thanks to the function *Image Arithmetic*. The goal of this manipulation is to keep only the particles which will be treated by the next function : the *Cross Correlation* comparing their slightly displacement between the two images of the couple.

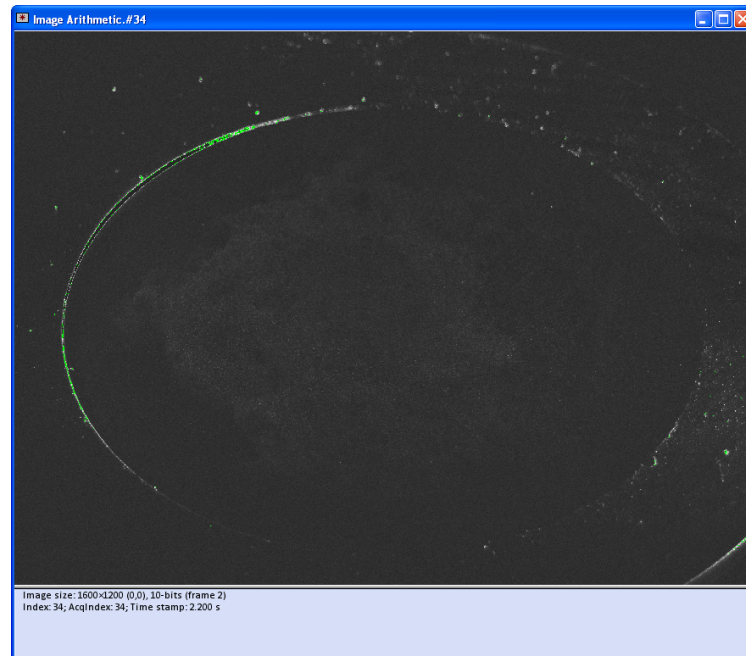
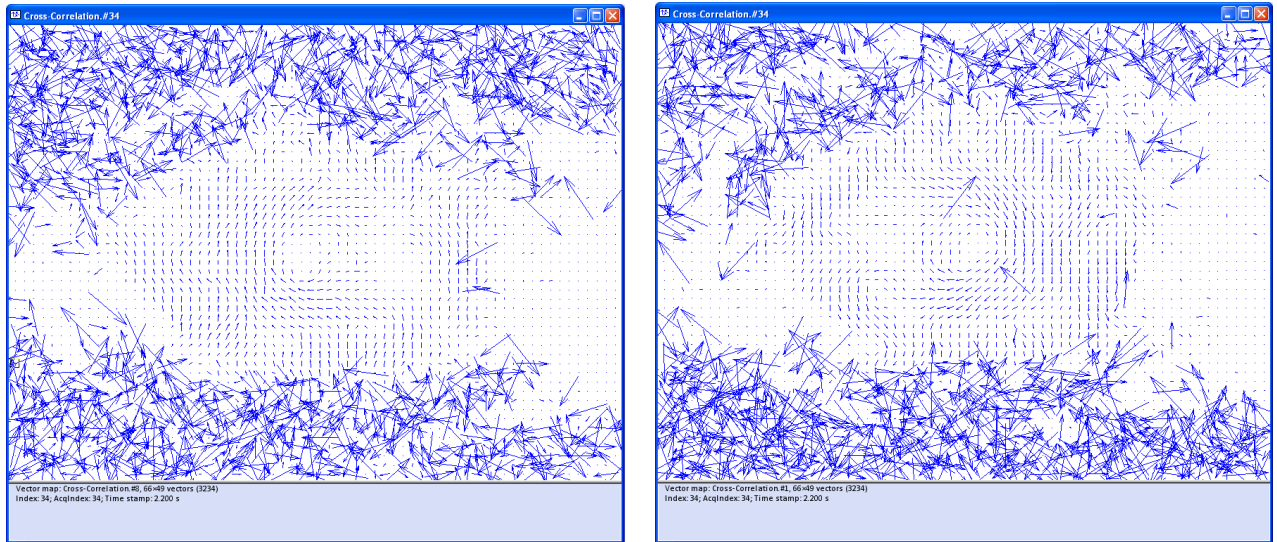


Figure 36: Isolated illuminated particles represented by this cloud in the center.

Essentially the *Cross Correlation* function statistically measures the degree of match between the two samples (the two images of the couple) in predefined interrogation windows (the image is discretized into many windows). The highest value in the correlation plane can then be used as a direct estimate of the particle image displacement. The vector of the local flow velocity (in the plane of the light sheet) is calculated taking into account the time delay between the two illuminations and the magnification factor of the image. This process is repeated for each interrogation window to build up the complete 2D velocity vector map. With a sufficient number of particle pairs (at least 20 is recommended) in the interrogation window the method is robust and works well even in moderately noisy situations. Each couple of images gives one single image representing a 2D vector map :



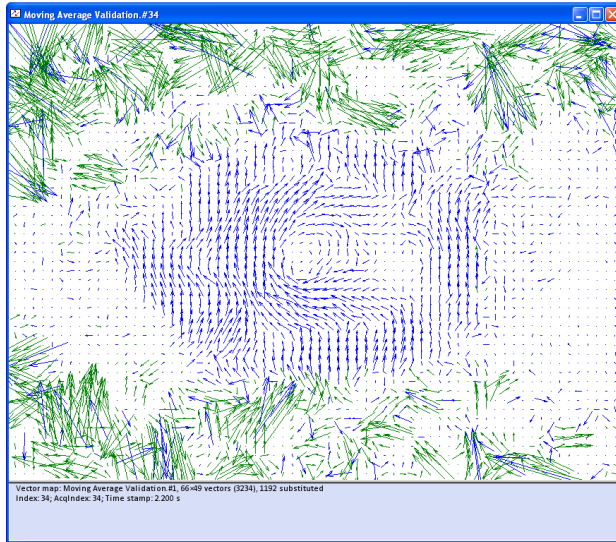
For the camera 1 at time = t

For the camera 2 at time = t

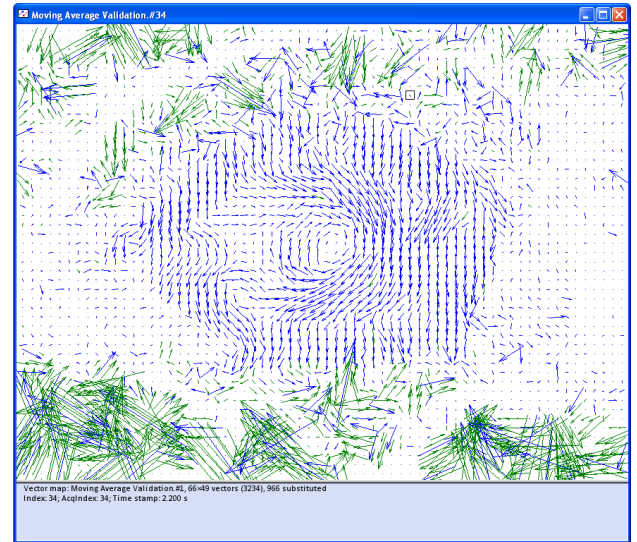
Figure 37: Cross correlation obtained for a couple of images and for each camera at the same time.

We can clearly see on the Figure 37 a clockwise recirculating motion created by the swirler. The longest and unordered arrows around this vortex are due to the lack of tracer particles. In fact the cross correlation does not see any correlation between the two images of the couple.

Then comes the *Moving Average Validation* function. This method is used to validate vector maps by comparing each vector with the average of other vectors in a defined neighborhood. Vectors that deviate too much from their neighbors can be replaced by the average of the neighbors as a reasonable estimate of true velocities. Therefore it “cleans” the cross-correlation and reconstruct a flow motion tidier. We can play on different parameters like the averaging area size (MxN), the acceptance factor (Ap) and the number of iterations (n). The new vector is calculated by local interpolation using iterations (within the averaging area), the acceptance factor is used to determine a spurious vector and shall be replaced by a “cleaner” vector (represented by the green vectors). We finally get the same number of images of the cross correlation but cleaned :



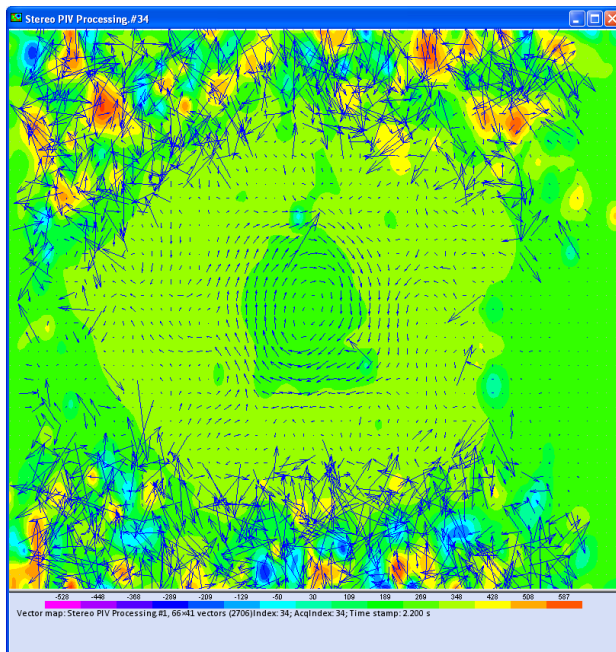
For the camera 1 at time = t



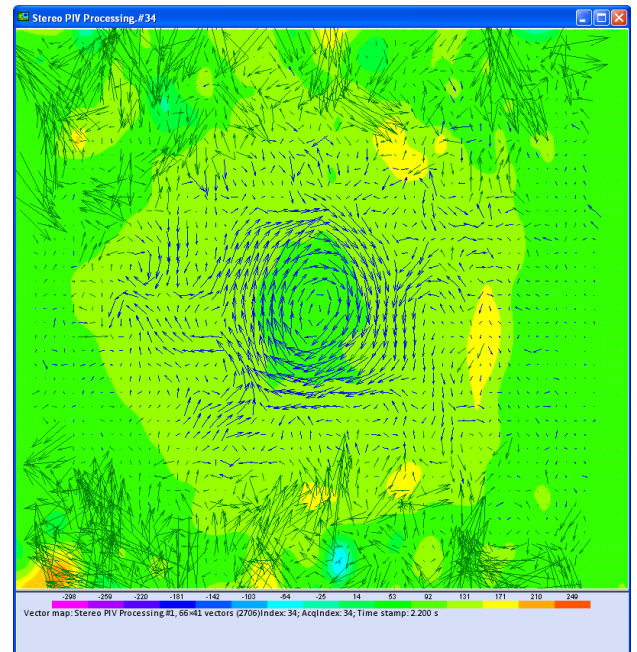
For the camera 2 at time = t

Figure 38: Moving average validation for each camera at the same time.

Then the *Stereo PIV Processing* is used. It consists in the pooling of the cross correlations from each camera at the same time t. The third velocity component is taken into account considering the calibration grid. We finally get (n-1) instantaneous 3D maps representation of the flow motion.



Without the moving average validation



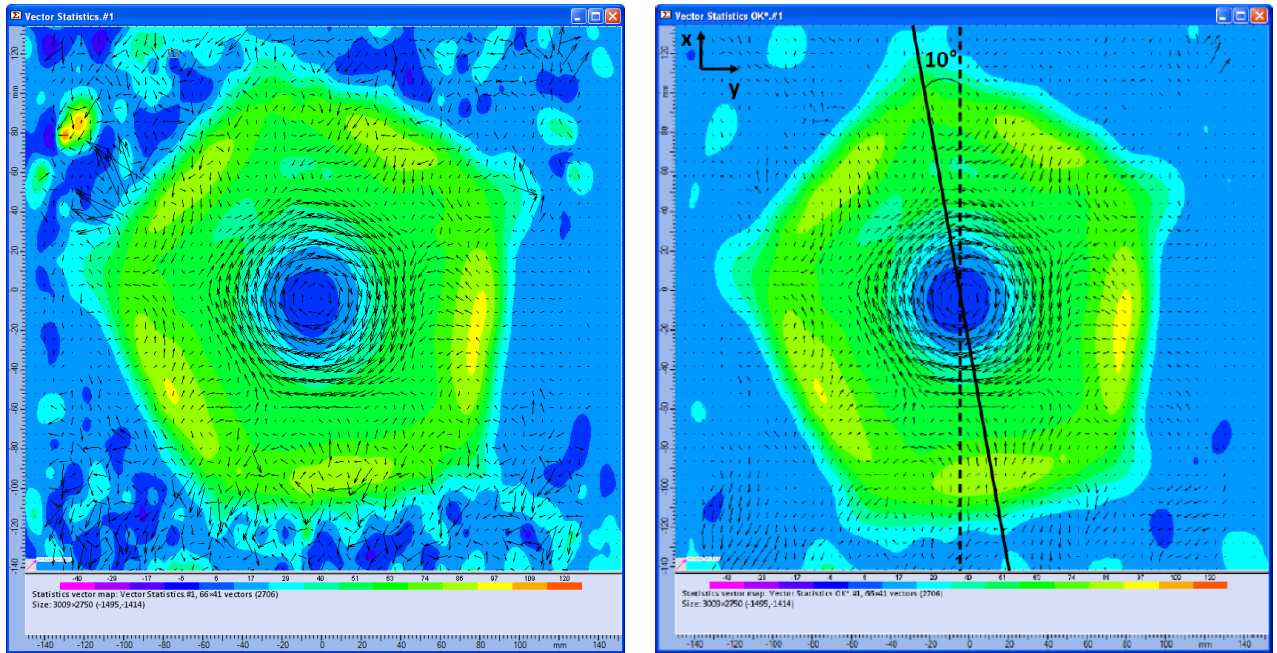
With the moving average validation

Figure 39: Stereo PIV Processing with and without the cleaned cross correlation.

We can see a cleaner motion of the vortex in the second case and the presence of the green corrected

arrows. We can also distinguish small vortexes around the main one. Note : the scale are not the same due to the corrupted velocity in the left frame.

And finally, we used a *Vector Statistics* function that compute the average of all the images from the *Stereo PIV Processing*. We finally get one image which is the mean 3D representation of the flow motion recorded by both cameras during a certain time.



Without the moving average validation

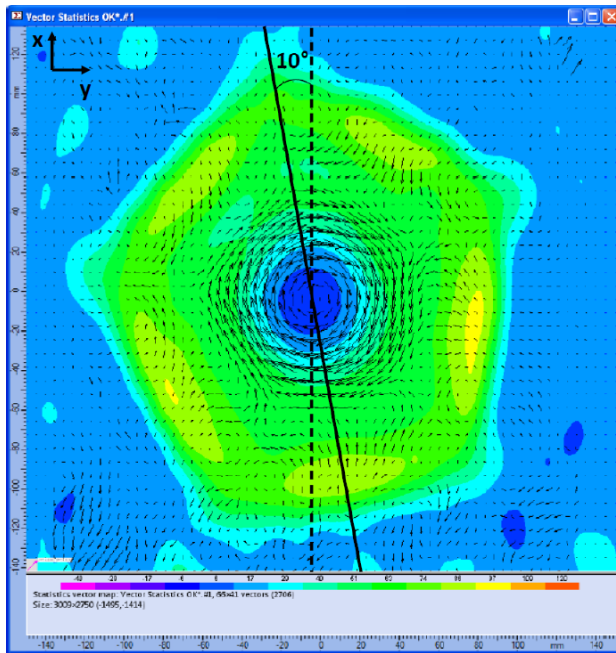
With the moving average validation

Figure 40: Mean representation of the flow recorded a certain time.

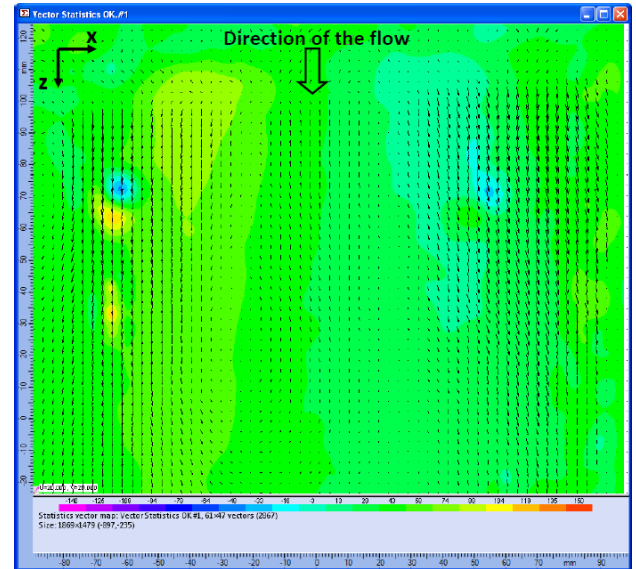
Then on these two ultimate maps, we can clearly see the advantageous effect of the function *Moving Average Validation*. Then, we followed exactly the same sequence for each measure according to the three air mass flow rates defined previously (in the Table 6). We will now present and confront each transverse and longitudinal measurements realized for each flow rate (considering now just the “cleaned” cross correlations). This way we will get a kind of identity card of the flow along two planes and will see the influence of the increase of flow velocity. All the transverse maps have been scaled in the same way and idem for the longitudinal ones. However, the software is weak for quantifying velocity, thus we are just interested in the flow motion and not about its velocity.

Due to the complexity of the assembly of the swirler, it was not exactly vertical respect to the vertical axis of the swirler. Then we had an angle shift between these two axis. This angle is useful for the post processing and will be considered for the new CFD analysis which will take into account the experimental configuration. The shift angle has been evaluated to  $10^\circ$  rotated clockwise respect to the vertical axis. Indeed, we will see that the longitudinal plane is not perfectly symmetric.

- Euler similitude :  $\dot{m} = 1.012 \text{ kg/s}$  :



Transverse map for  $\dot{m} = 1.012 \text{ kg/s}$



Longitudinal map for  $\dot{m} = 1.012 \text{ kg/s}$

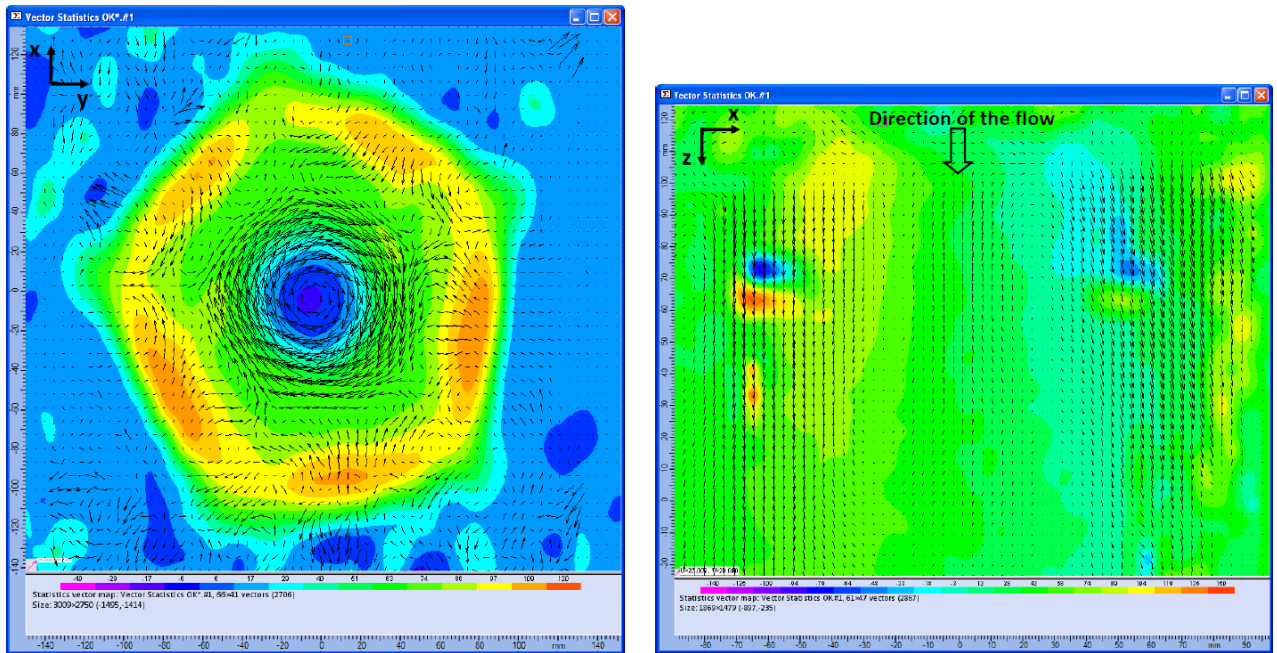
Figure 41: 3D average maps along the two measurement planes for  $\dot{m} = 1.012 \text{ kg/s}$ .

The transverse map shows clearly the huge clockwise rotating vortex in the middle which has the diameter of the swirler (as the measure has been taken very close to its outlet) and surrounded by small vortexes. We can also notice that in the center of this vortex, the flow goes back with a negative velocity (along the z axis).

On the longitudinal map (the outlet of the swirler is up and the flow goes down), the flow profile is confirmed by the fact that in the center, we can see the flow going back toward the swirler (corresponding to the blue shades in the center of the transverse map). We can also distinguish that the flow is faster on the left side than on the right side (along the y axis). In fact we can imagine that the longitudinal plane corresponds to a vertical line passing in the middle of the transverse map to see the correspondence.

As it can be seen on the left hand image of the Figure 41, we represented the location of the longitudinal plane by the dashed line and the symmetry axis of the component by the straight line.

- Velocity similitude :  $\dot{m} = 1.442 \text{ kg/s}$  :



Transverse map for  $\dot{m} = 1.442 \text{ kg/s}$

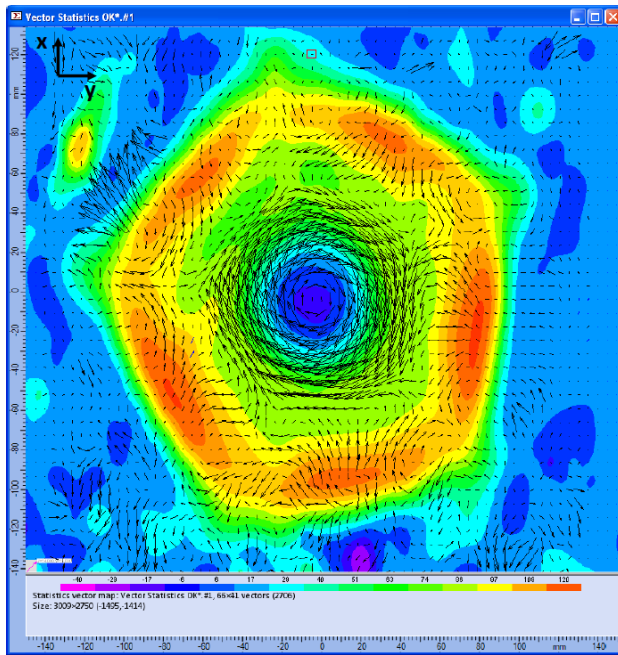
Longitudinal map for  $\dot{m} = 1.442 \text{ kg/s}$

Figure 42: 3D average maps along the two measurement planes for  $\dot{m} = 1.442 \text{ kg/s}$ .

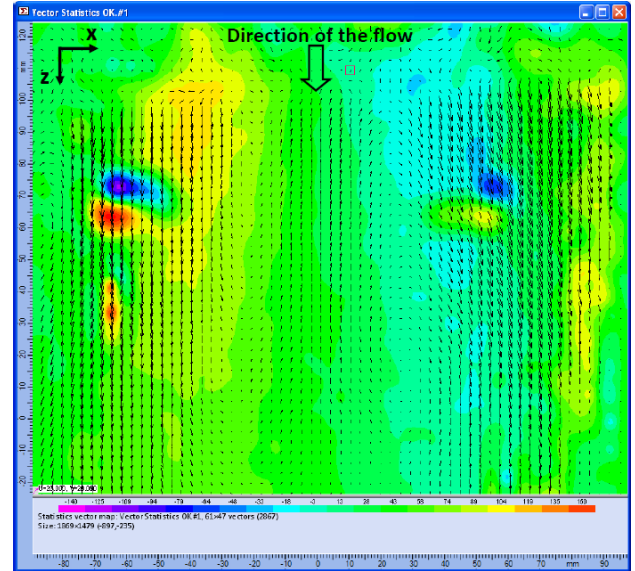
On that transverse map, we can see the worsening of the central vortex. The rise of velocity also amplifies the return of the flow upstream. We can also distinguish the amplification of the velocity around the swirler which correspond to the empty holes of the fuel nozzles and let the air passing faster.

Regarding to the longitudinal plane, the distinction of the two different velocities becomes clearer on left and right and creates a clear shear. We can also notice an appearing secondary stationary vortex on the left around the y axis (blue and red spots on the left of the image). The non symmetry of this vortex is due to the non symmetry of the swirler, as explained for the previous flow rate case.

- Reynolds similitude :  $\dot{m} = 1.62 \text{ kg/s}$  :



Transverse map for  $\dot{m} = 1.62 \text{ kg/s}$



Longitudinal map for  $\dot{m} = 1.62 \text{ kg/s}$

Figure 43: 3D average maps along the two measurement planes for  $\dot{m} = 1.62 \text{ kg/s}$ .

To be more precise, we put on a same line the three transverse and longitudinal maps for an easier confront. On these, we can clearly see that the phenomenons defined previously are amplified due to the increasing velocity of the flow. In fact, the swirl motion of the transverse map becomes very powerful and the turning down flow in the center still becomes important. Moreover, the swirling motion of the longitudinal case increase of intensity.

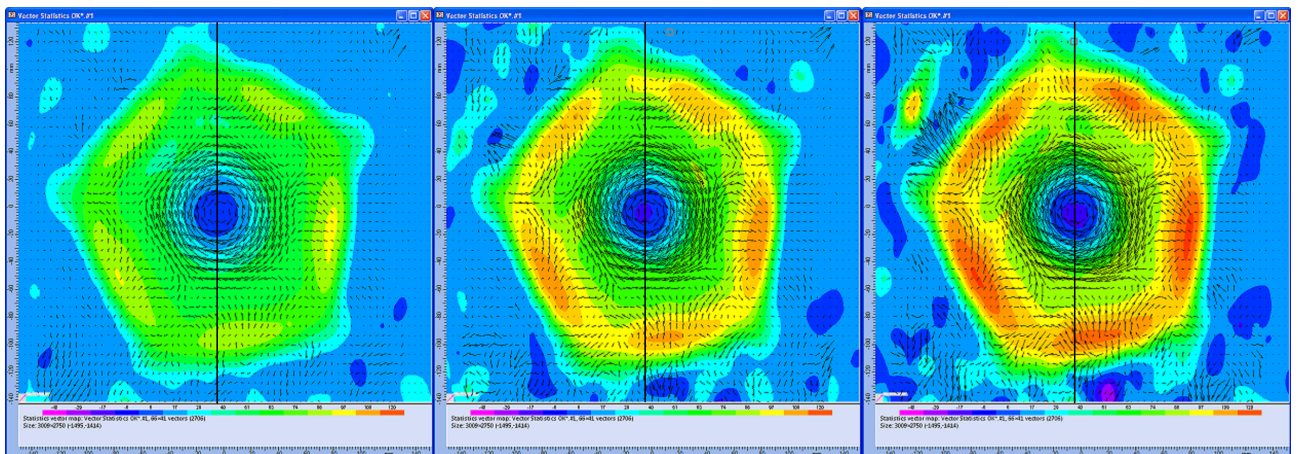


Figure 44: Transverse average maps for the three air mass flow rates.

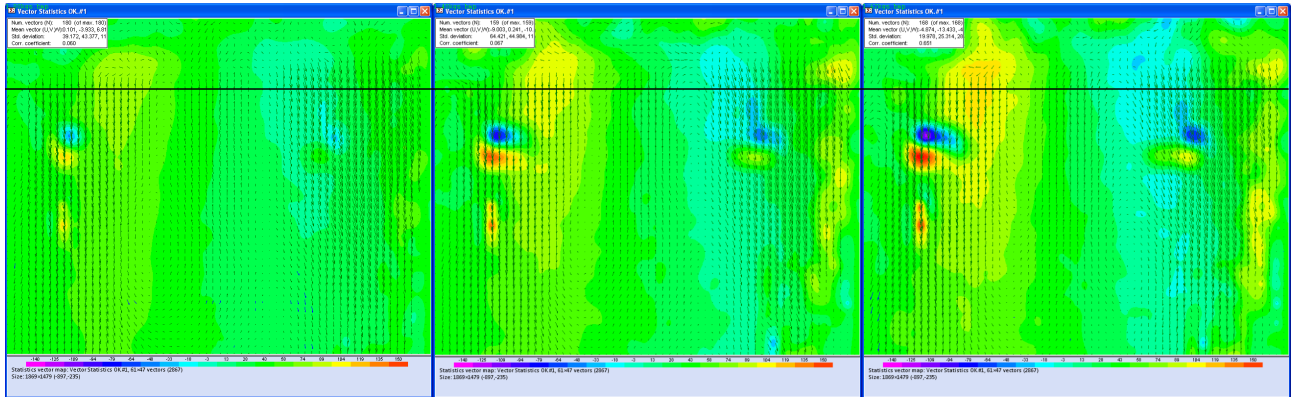


Figure 45: Longitudinal average maps for the three air mass flow rates.

Thanks to the color scale we can see well the areas of recirculation and its evolution which are stronger as the maximum air flow rate inlet increase. (Note : The black lines on both panoramic images represent the positions of the profile plots presented below).

Then we computed the profile plots of the velocity for the two planes of measurement (Figure 46 and 47). We took the velocity in the z direction (W) of the transverse measurement plane corresponding to the velocity in the z direction of the longitudinal plane (V) :

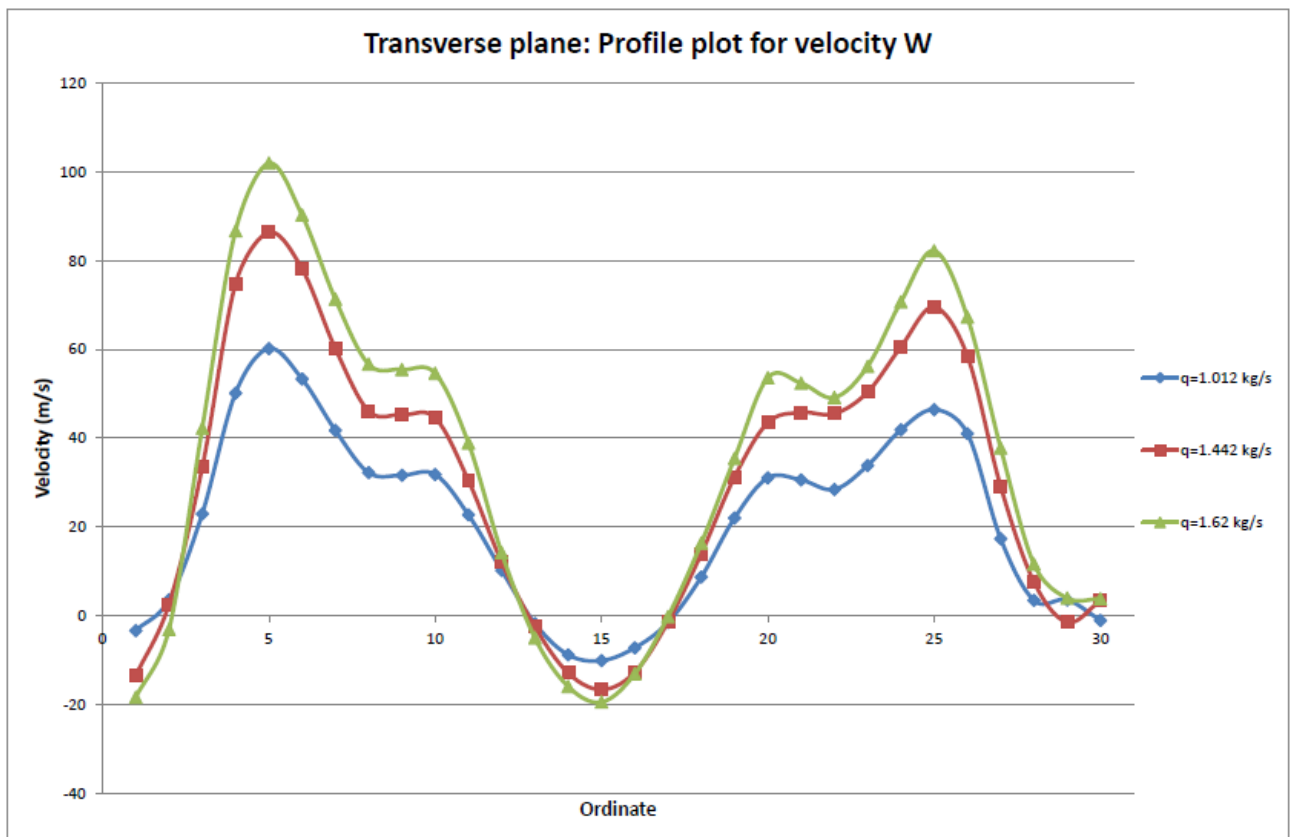


Figure 46: Profile plot of the velocity W for the transverse measurement.

So it can be clearly seen the symmetry on both side of the central swirler through the positive velocity and the negative velocity of the turning back flow in front of the swirler. We can note that the profile is not exactly symmetric respect to the center because of the asymmetry of the swirler. Then we computed the same corresponding profile for the longitudinal plane:

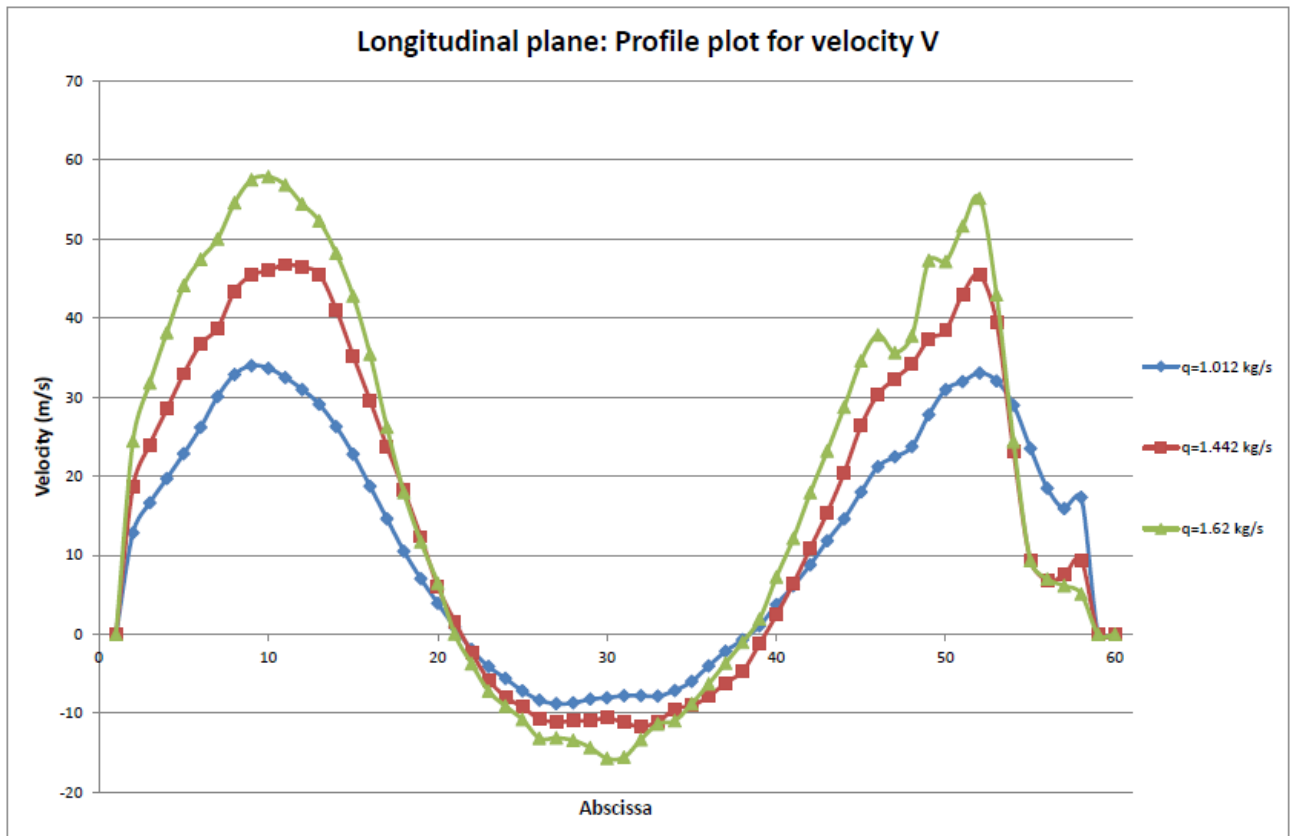


Figure 47: Profile plot of the velocity V for the longitudinal measurement.

These two maps represents the “same” velocity profiles. One for a horizontal line located at the beginning of the longitudinal plan and a vertical line in the middle of the transverse one. We can clearly note the same trend but not exactly the same value. This is due to the fact that the two velocity profiles was not exactly define at the same location for both measures because the transverse measure was right after the outlet of the venturi instead of the longitudinal measure has been taken from a little bit downstream because of the cylinder with the windows. We can also observe that the trend remains the same as the velocity of the fluid increase.

Finally, we have used a function of the software called *dewarping*. It allows to (redresser) the image seen by one camera in order to cancel the perspective so that the component could be seen from the front. We superposed on it one of the vectorial field obtained previously to check the accuracy or plausibility of the result (for  $\dot{m} = 1.442 \text{ kg}\cdot\text{s}^{-1}$ ) :

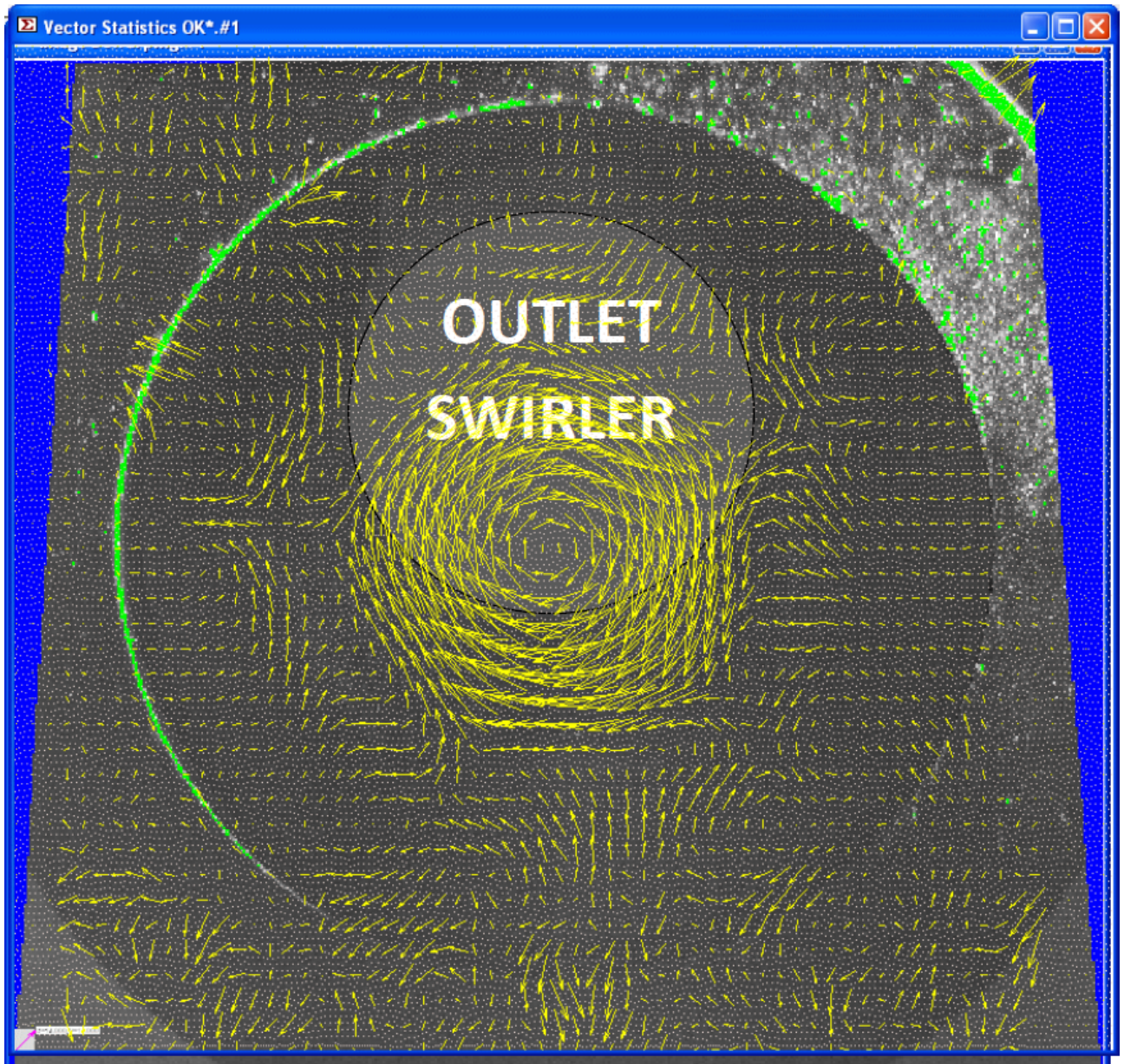


Figure 48: Overlaying of the swirler with the trasverse vectorial map.

In fact we can see the central swirling motion surrounded by small vortexes all around with the goal to create an optimal and homogeneous mixing air/fuel.

## 8 Conclusion

This training course has been realized in an Italian company, one of the leader in the energy production field. During six months, we have led an experimental project inside the combustion group of the research and development department to understand the air flow structure developed by a burner.

We have applied our knowledge directly on a complex technology for an industrial application and it has been shown that the theoretical and experimental differs. Indeed, we have seen that the engineer takes into account in his (her) work all the unforeseen which could succeed all along the project. He has to discuss, decide and plan with all the team in sort of achieving the objectives. It is in the good organization (schedule, management, results...) that depends the progress of the project.

This training course allowed us to learn new techniques to analyze a flow motion and to take the first step in the industry. Engineer is a tough job which asks good qualities in term of management, he has a lot of responsibilities.

It was very interesting to participate to a concrete and practical project in which the results will allow to understand how react components which downstream will improve the technology in term of the reduction of the pollutant emissions.

The combustion field is a very complex and interesting part of the mechanic in which there is so much work to do to improve its process; the PIV experiment is just one technique which allow to understand better the phenomenons. It has been a rewarding job to work with this advanced technique which is very helpful and essential for the development or understanding of such a component and above all to get satisfying and acceptable results.

## 8.1 References

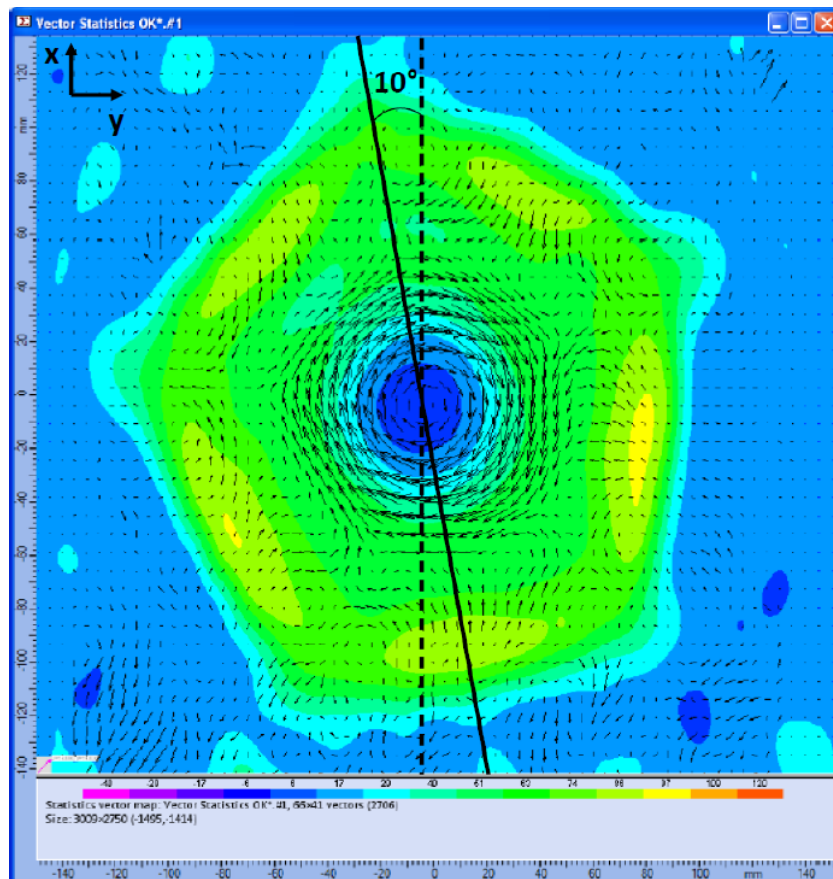
- [1] RAFFEL, Markus, Particle image velocimetry, Springer.
- [2] IDELCHIK, Ivan.E, Handbook of hydraulic resistance, Hemisphere Corporation, 1986.
- [3] OHKUBO, Yoichiro, Low NOx Combustion Technology, RD Review of Toyota CRDL Vol 41 No 1.
- [4] RICHARDS, George, Combustion strategies for syngas and High- Hydrogen fuel, The gas turbine handbook, 2006.
- [5] PRASAD, Ajay K, Particle Image Velocimetry, Current Science, Vol. 79, No. 1, 10 July 2000.
- [6] WESTERWEEL, J, Digital Particle Image Velocimetry - Theory and Application. PhD., Delft University of Technology, The Netherlands, 1993.
- [7] TONDDAST-NAVAEI, Ali, Acoustic Particle Image Velocimetry - Development and Applications.
- [8] Powerpoints ANSALDO ENERGIA for PIV, laser security and turbines' principle.
- [9] STANISLAS, Particle Image Velocimetry; Progress towards Industrial Application, 2000.
- [10] CORREA, S.M, A review of NOx formation under gas-turbine combustion conditions vol. 87, No1-6, pp. 329-362, Combustion science and technology, Taylor and Francis, 1993.
- [11] MELLOR, A.M, Gas turbine engine pollution Volume 1, Issues 2-3, 1976, Pages 111-133, Progress in Energy and Combustion Science, ELSEVIER, 2003.
- [12] [www.dantecdynamics.com/](http://www.dantecdynamics.com/)
- [13] [http://master-efe.mmpmsi.fr/telechargement/slides\\_cabot\\_combaero\\_masterefe.pdf](http://master-efe.mmpmsi.fr/telechargement/slides_cabot_combaero_masterefe.pdf)

## A Appendix

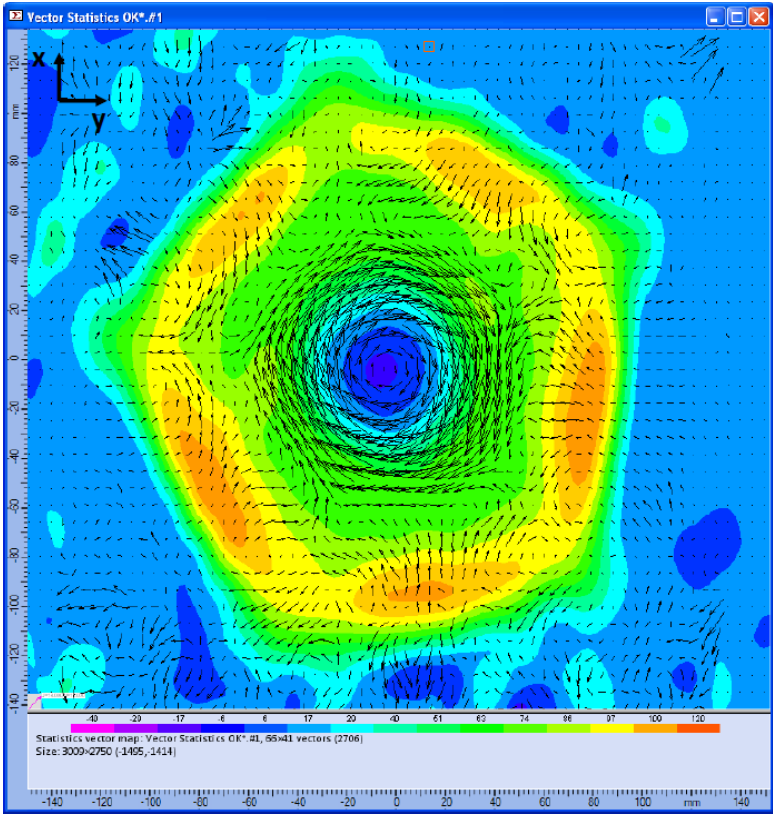
### Table of appendixes :

- Appendix A: transverse map for  $\dot{m} = 1.012 \text{ kg.s}^{-1}$ ;
- Appendix B: transverse map for  $\dot{m} = 1.442 \text{ kg.s}^{-1}$ ;
- Appendix C: transverse map for  $\dot{m} = 1.62 \text{ kg.s}^{-1}$ ;
- Appendix D: longitudinal map for  $\dot{m} = 1.012 \text{ kg.s}^{-1}$ ;
- Appendix E: longitudinal map for  $\dot{m} = 1.442 \text{ kg.s}^{-1}$ ;
- Appendix F: longitudinal map for  $\dot{m} = 1.62 \text{ kg.s}^{-1}$ ;
- Appendix G: light spectrum;
- Appendix H: transverse vectorial map for  $\dot{m} = 1.012 \text{ kg.s}^{-1}$ ;
- Appendix I: transverse vectorial map for  $\dot{m} = 1.442 \text{ kg.s}^{-1}$ ;
- Appendix J: transverse vectorial map for  $\dot{m} = 1.62 \text{ kg.s}^{-1}$ .

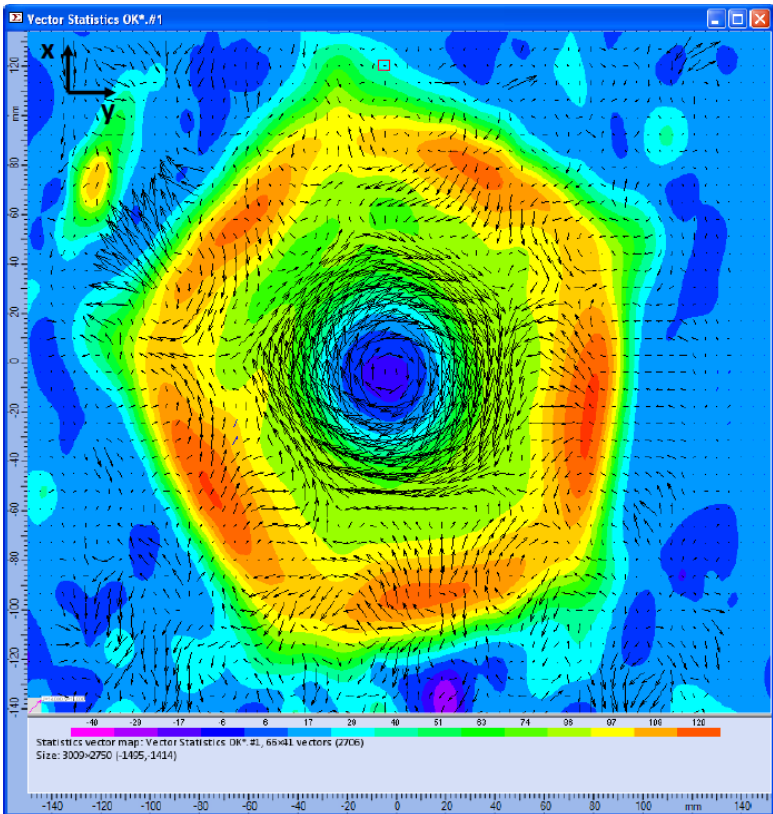
**Appendix A:** transverse map for  $\dot{m} = 1.012 \text{ kg.s}^{-1}$



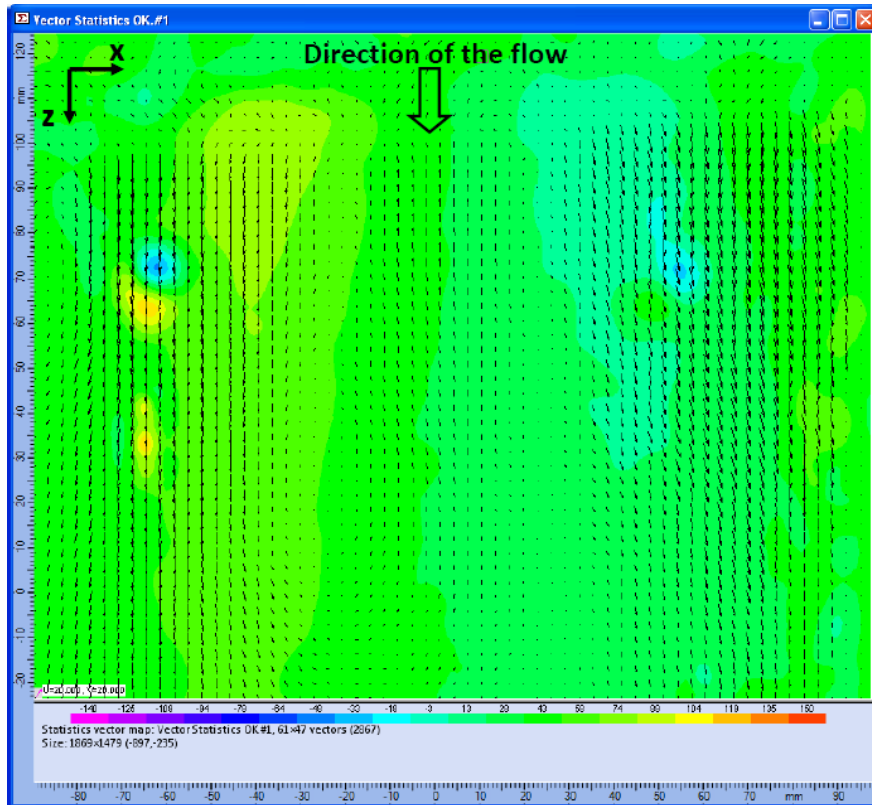
Appendix B: transverse map for  $\dot{m} = 1.442 \text{ kg}\cdot\text{s}^{-1}$



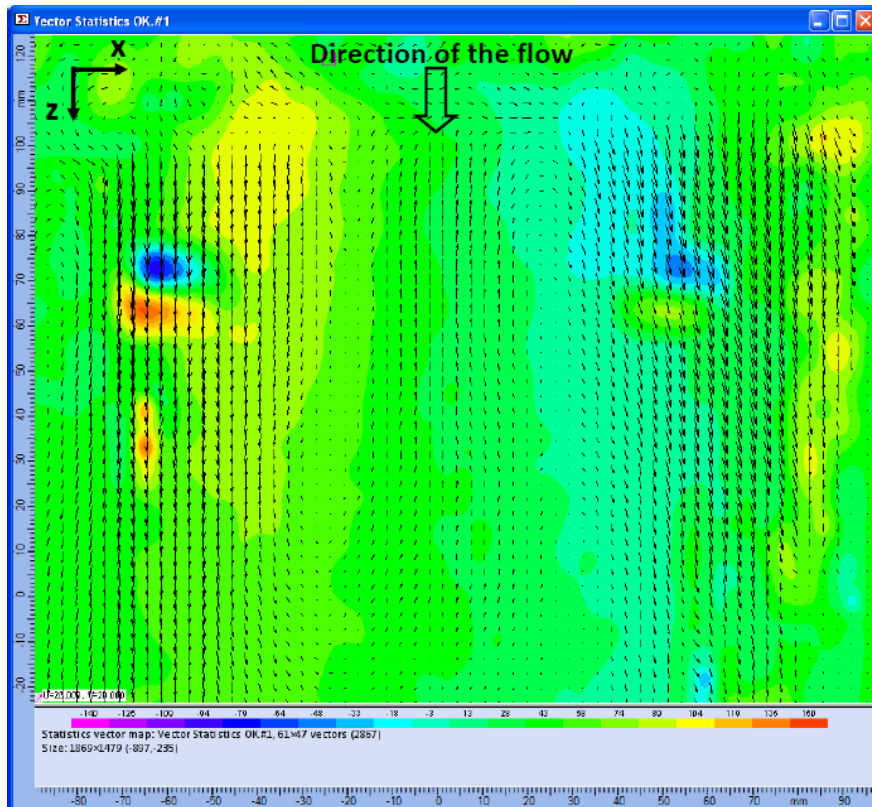
Appendix C: transverse map for  $\dot{m} = 1.62 \text{ kg}\cdot\text{s}^{-1}$



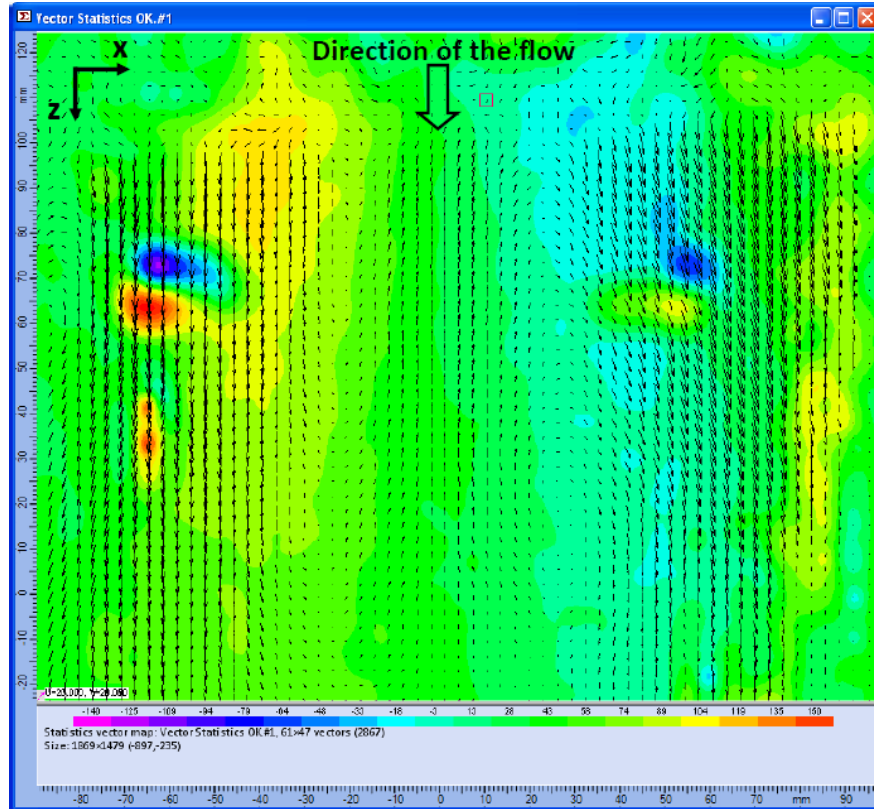
Appendix D: longitudinal map for  $\dot{m} = 1.012 \text{ kg}\cdot\text{s}^{-1}$



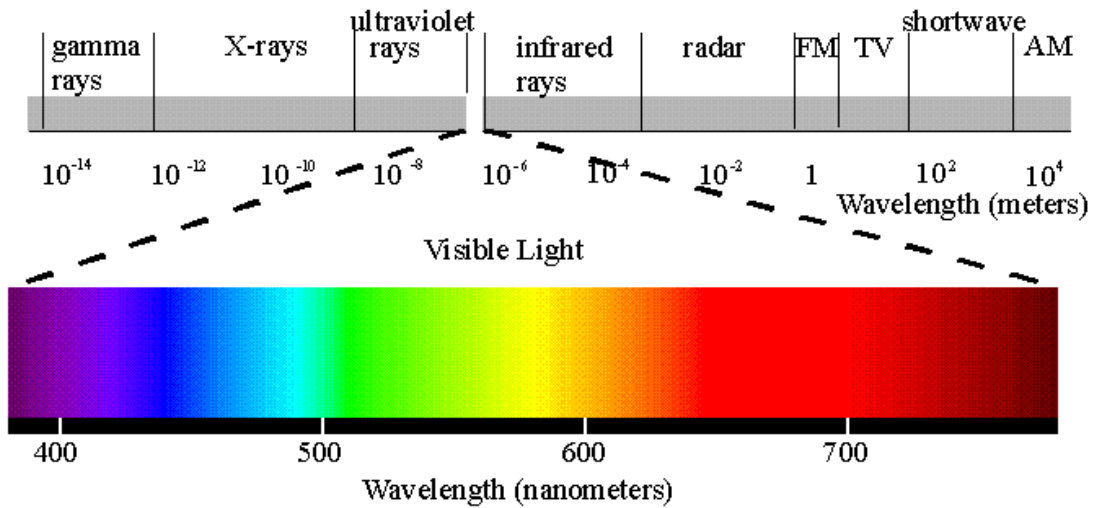
Appendix E: longitudinal map for  $\dot{m} = 1.442 \text{ kg}\cdot\text{s}^{-1}$



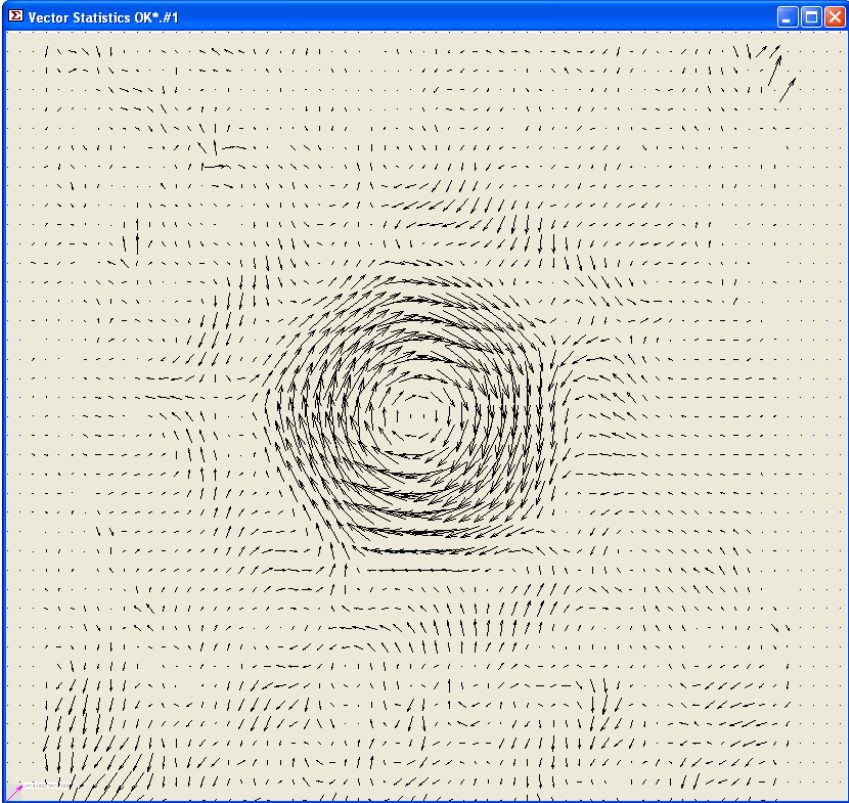
Appendix F: longitudinal map for  $\dot{m} = 1.62 \text{ kg}\cdot\text{s}^{-1}$



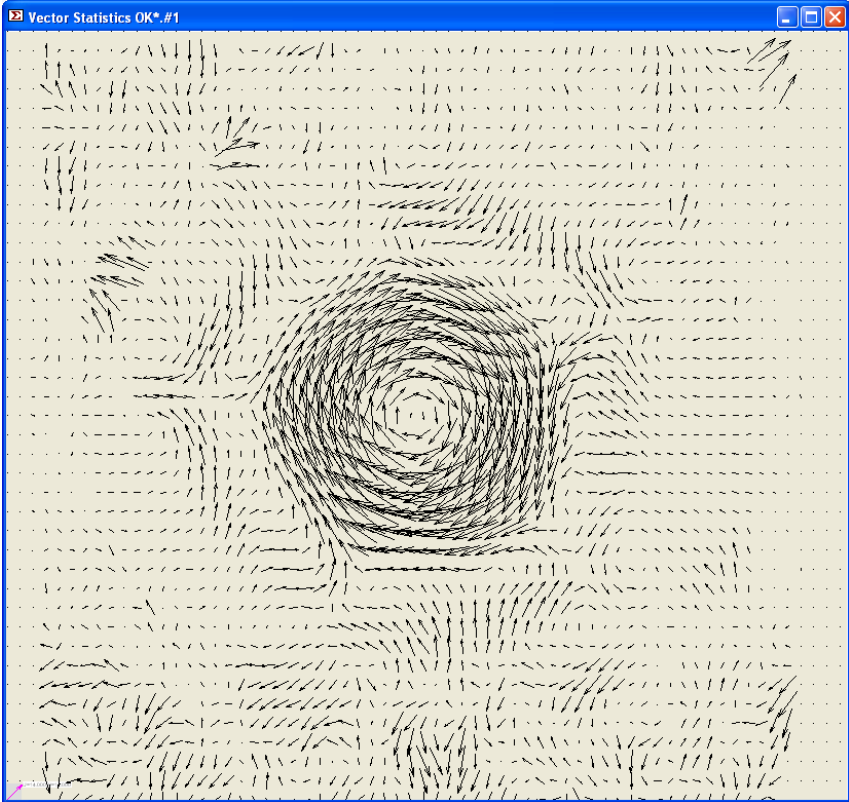
Appendix G: light spectrum



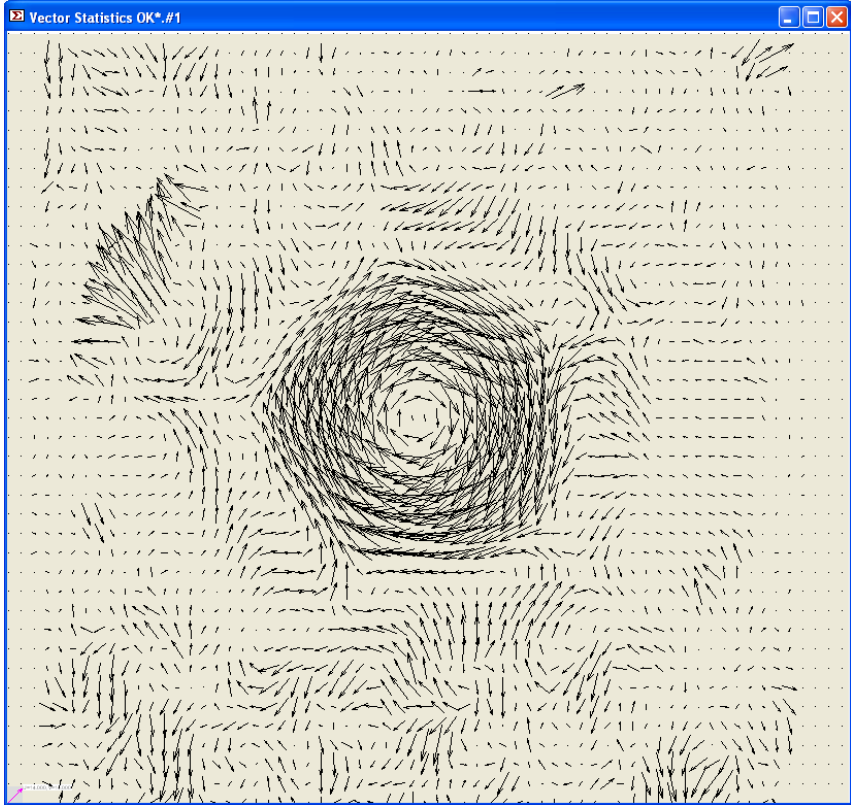
**Appendix H:** transverse vectorial map for  $\dot{m} = 1.012 \text{ kg}\cdot\text{s}^{-1}$



**Appendix I:** transverse vectorial map for  $\dot{m} = 1.442 \text{ kg}\cdot\text{s}^{-1}$



**Appendix J:** transverse vectorial map for  $\dot{m} = 1.62 \text{ kg}\cdot\text{s}^{-1}$



**Abstract :**

This engineering internship/Thesis allowed us to apply the knowledge acquired during these two years at the Ecole Polytechnique of the University of Orleans and this year at the University of Genoa. This internship has been realized in the Italian company Ansaldo Energia, one of the worldwide leader for power plant turbines. We discovered the PIV technique (Particle Image Velocimetry) which allows to visualize a flow structure and to measure its velocity. We used it on a swirler which had the goal to create an homogeneous mixture air/fuel into a combustion chamber. Then we could apply our experimental and theoretical skills to interpret the data, to anticipate and understand the fluid-dynamics phenomenon.

**Résumé :**

Ce stage/Master Thesis d'ingénieur nous aura permis de mettre en application les connaissances acquises durant nos deux premières années à l'Ecole Polytechnique de l'Université d'Orléans ainsi qu'au cours de cette dernière année auprès de l'Université de Gênes. Ce stage a été réalisé au sein de l'entreprise italienne Ansaldo Energia, un des leaders mondiaux élaborant des turbines pour la production d'électricité. Nous avons pu y découvrir la technique PIV (Particle Image Velocimetry) permettant de visualiser la structure d'un flux et d'en mesurer sa vitesse suivant deux ou trois directions de l'espace. Nous l'avons donc appliquée à un swirler permettant de créer un mélange homogène air/carburant dans une chambre de combustion. Nous avons donc pu mettre en application nos compétences expérimentales ainsi que théorique pour l'interprétation des données, l'anticipation et la compréhension des phénomènes fluide-dynamiques.

**Riassunto :**

Questo tirocinio/Master Tesi ci ha permesso di applicare le conoscenze acquisite durante i nostri primi due anni all'Ecole Polytechnique dell'Università di Orleans e durante questo ultimo anno presso l'Università di Genova. Questo tirocinio è stato realizzato in seno all'azienda italiana Ansaldo Energia, uno dei leader mondiali nell'elaborazione delle turbine per la produzione di elettricità. Abbiamo potuto così applicare la tecnica PIV (Particle Image Velocimetry) permettendoci di visualizzare la struttura di un flusso e di misurarne la sua velocità rispetto a due o tre direzioni dello spazio. Di conseguenza l'abbiamo applicata ad uno swirler che consente di creare una miscela omogenea aria/combustibile in una camera di combustione. Abbiamo quindi potuto mettere in pratica tanto le nostre competenze sperimentali quanto quelle teoriche per l'interpretazione dei dati, la previsione e la comprensione dei fenomeni fluidodinamici.